



Politecnico di Torino  
Master degree in Nanotechnologies for ICTs

# Integration of dielectrophoretic trapping on a glass suspended microchannel resonator

Relator: Prof. Carlo Ricciardi

Co-relators: Dr. Stefano Stassi, Dr. Roberta Calmo

Author: Lorenzo Ranieri

March 28, 2022



## Abstract

In recent years, systems based on micro and nanoscale resonators have shown their potential as mass sensors with unparalleled sensitivity: yoctogram mass resolution has been reached using the smallest carbon nanotube resonators, proportionally decreasing with increasing resonator mass.

The measurements obtained with these devices have the additional advantage of being intrinsically time resolved, as the resonator response is, at any given time, directly linked to the mass on the resonator. These features make them well-suited for the study of biological samples and ultimately processes (the latter is done by monitoring mass changes in the system, an example use case would be measuring the concentration changes of a specific protein during a cellular reaction); however this introduces the need to work in liquid, which drastically reduces the resonator's sensitivity because of the fluid's damping.

The suspended microchannel resonator (SMR) approach removes most of the viscous damping from the fluid by confining the solution under analysis *inside* the resonator, which is now a microchannel that can be suspended in air or vacuum (hence the name); SMRs can be integrated in a more complex microfluidic system to finely control the samples that pass through the resonator and more of them can be arrayed to perform more complex measurements or increase throughput.

In order to keep the sample within the resonator for longer measurements (necessary for example to study mass variations during cellular processes), various techniques have been documented: functionalizing the surface of the channel to promote selective chemisorption of the samples or exploiting the channel geometry to trap them or slow them down are examples.

In this work we show the implementation of dielectrophoresis (DEP) as a trapping method in a glass SMR device, with a different configuration than usually seen in literature: the electrodes are fabricated on top of the device and do not contact the liquid.

While many trapping techniques used with SMR devices require a complex fabrication process resulting in higher costs and a reduced range of possible designs, this device was made with a relatively fast and cost-effective process thanks to the combination of a 3D-resolved femtosecond laser direct writing process for the channels and SMR and an ion beam etching process only slightly modified from the standard ones for the electrodes.

The mechanical properties and particle detection capabilities of the device were tested first without DEP, then the trapping and sensing capabilities of the SMR device with the new DEP approach were confirmed.

# Contents

<b>Abstract</b>	<b>ii</b>
<b>1 Fundamentals of microresonators</b>	<b>2</b>
1.1 Bending oscillations . . . . .	2
1.2 Driven damped oscillator . . . . .	4
1.3 Mass sensing and responsivity . . . . .	5
<b>2 Suspended Microchannel Resonators</b>	<b>6</b>
<b>3 Particle trapping with Dielectrophoresis (DEP)</b>	<b>7</b>
3.1 General working principle . . . . .	7
3.2 DEP force . . . . .	7
3.3 DEP with an AC field . . . . .	7
3.4 DEP trapping in the SMR device . . . . .	8
3.5 Comparison with other trapping approaches for SMR . . . . .	9
<b>4 Device specifics and fabrication process</b>	<b>10</b>
4.1 Design choices . . . . .	10
4.1.1 Suspended bridge . . . . .	10
4.1.2 Microfluidics . . . . .	11
4.1.3 Electrodes for DEP . . . . .	11
4.2 Fabrication process . . . . .	11
4.2.1 Femtosecond laser machining of transparent materials . . . . .	11
4.2.2 Fabrication process of the SMR-DEP device . . . . .	13
<b>5 Measurement set-up</b>	<b>17</b>
5.1 Sample positioning and isolation from vibrations . . . . .	17
5.2 Microfluidics setup . . . . .	17
5.3 Actuation method and read-out system . . . . .	18
5.4 Signal processing and control system . . . . .	18
5.5 DEP setup . . . . .	18
<b>6 Device characterization and measurements</b>	<b>19</b>
6.1 Resonance spectra - Air . . . . .	19
6.2 Resonance spectra - Liquids . . . . .	19
6.3 Allan Deviation . . . . .	24
6.4 Flow-through measurements with particles . . . . .	25
6.5 DEP tests with particles . . . . .	30
<b>7 Conclusions</b>	<b>35</b>
<b>Appendix: Post-processing with codes</b>	<b>37</b>
Common scripts . . . . .	37
Allan deviation . . . . .	38
Flow-through measurements . . . . .	41
DEP measurements . . . . .	50
<b>References</b>	<b>57</b>

# 1 Fundamentals of microresonators

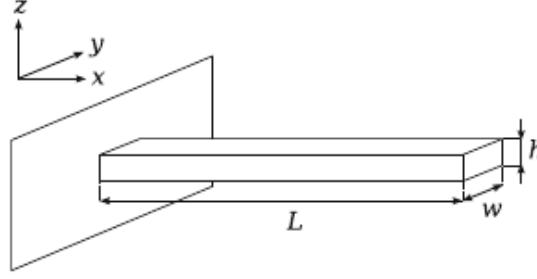
## 1.1 Bending oscillations

Our measurement focuses on the bending vibration of the resonating bridge, and the way they change in response to a mass.

If the beam is slender enough ( $L/h \gg 1$ ) and we can neglect rotational inertia and shear deformation, the bending behaviour of beams is modelled by the *Euler-Bernoulli beam theory*, which, by subdividing the beam in infinitesimal sections and solving the force equilibrium for small deflections and a linear elastic material, obtains the following equation of motion [1]:

$$\rho A \frac{\partial^2 u(x, t)}{\partial t^2} + EI_y \frac{\partial^4 u(x, t)}{\partial x^4} = 0, \quad (1)$$

where  $\rho$  is the density,  $A$  is the section of the beam,  $E$  is its Young's modulus and  $I_y$  is the second moment of area ( $I_y =$ ) relative to the  $y$  (See Fig. 1) axis.



**Figure 1:** Reference for the axes and beam dimensions used in this section [1].

The general form [1] for the eigenmodes of (1) is:

$$U_n(x) = a_n \cos(\beta_n x) + b_n \sin(\beta_n x) + c_n \cosh(\beta_n x) + d_n \sinh(\beta_n x) \quad (2)$$

which allows us to rewrite (1) as

$$-\rho A \omega^2 u(x, t) + EI_y \beta_n^4 u(x, t) = 0, \quad (3)$$

$$\text{with } u(x, t) = \sum_{n=1}^{\infty} U_n(x) \cos(\omega t). \quad (4)$$

From (3) we can obtain the dispersion relationship for the resonance frequency  $\Omega$ :

$$\Omega = \omega = \beta_n^2 \sqrt{\frac{EI_y}{\rho A}} \quad (5)$$

The boundary conditions [1] for a double clamped beam are:

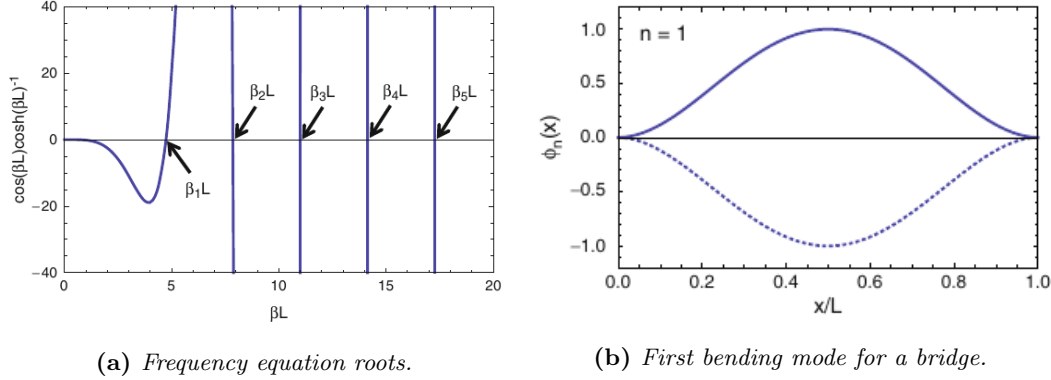
$$U_n(0) = U_n(L) = \frac{\partial}{\partial x} U_n(0) = \frac{\partial}{\partial x} U_n(L) = 0. \quad (6)$$

The linear system obtained by applying these conditions to (3) has nontrivial solutions for (Fig.2a plots the frequency equation and shows its roots):

$$\cos(\beta_n x) \cosh(\beta_n x) + 1 = 0, \quad (7)$$

with solutions for the wavenumbers  $\beta_n$

$$\begin{aligned} \beta_n L &\simeq 4.7300, 7.8532, 10.9956 \quad \text{for } n = 1, 2, 3; \\ \beta_n L &\sim (2n + 1)\pi/2 \quad \text{for } n \gg 3 \end{aligned} \quad (8)$$



**Figure 2:** Solutions for the bending vibrations of a bridge [1].

After solving the system we obtain the normalized eigenmodes  $\phi_n(x)$  from (2):

$$\begin{aligned} \phi_n(x) &= \frac{U_n(x)}{\|U_n(x)\|} = \alpha \left[ \cos \beta_n x - \cosh \beta_n x - \frac{\cos \beta_n L - \cosh \beta_n L}{\sin \beta_n L - \sinh \beta_n L} (\sin \beta_n x - \sinh \beta_n x) \right] \\ \text{with } \begin{cases} \alpha \simeq 0.6297, 0.6626, 0.7112 & \text{for } n = 1, 2, 3 \\ \alpha \sim 1/\sqrt{2} & \text{for } n \gg 3 \end{cases} \end{aligned} \quad (9)$$

We are only interested in the first mode, for which we summarize the eigenvalue and eigenmode (Fig.2b) here:

$$\begin{aligned} \Omega_1 &= \beta_1^2 \sqrt{\frac{EI_y}{\rho A}} \simeq \left( \frac{4.7300}{L} \right)^2 \sqrt{\frac{EI_y}{\rho A}}; \\ \phi_1(x) &\simeq 0.6297 \left[ \cos \left( 4.7300 \frac{x}{L} \right) - \cosh \left( 4.7300 \frac{x}{L} \right) - 0.9825 \left( \sin \left( 4.7300 \frac{x}{L} \right) - \sinh \left( 4.7300 \frac{x}{L} \right) \right) \right] \end{aligned} \quad (10)$$

**Effective parameters** To study the dynamic behaviour of the resonance, we simplify the system as a harmonic oscillator with the same resonance

$$\Omega_n = \sqrt{\frac{k_{eff,n}}{m_{eff,n}}} \quad (11)$$

where the *effective parameters*  $k_{eff,n}$  and  $m_{eff,n}$  can be derived from the complete model.

In the case of a bridge in bending vibration, the following values can be obtained for the effective parameters [1]:

$$m_{eff} = \frac{1}{2} m_0; \quad k_{eff,n} = \Omega_n^2 m_{eff} \quad (12)$$

## 1.2 Driven damped oscillator

Starting from the harmonic oscillator simplification we can expand the model by considering a damping force and piezoelectric actuation of the chip:

$$F_{damping} = -c\dot{z}; \quad z_{drive}(\omega, t) = z_{drive,0}e^{i\omega t} \quad (13)$$

where  $z$  is the oscillator displacement and  $z_{drive}$  is the driving oscillation.

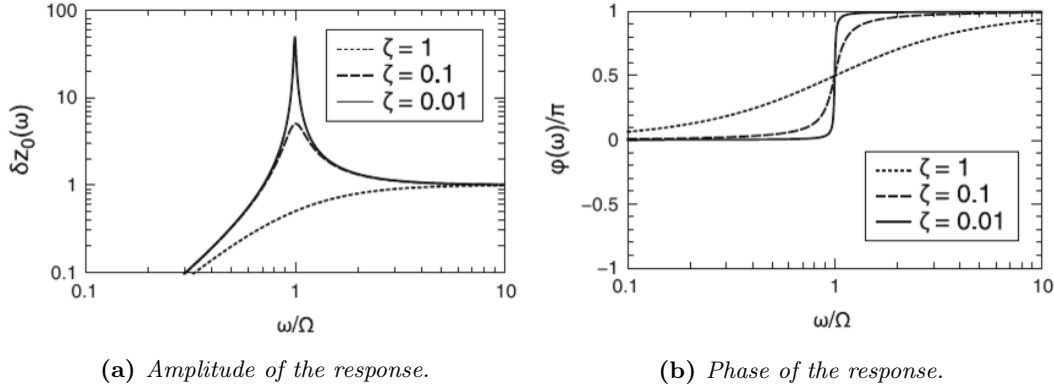
The resulting differential equation for the system is:

$$m_{eff}(\ddot{z} - \ddot{z}_{drive}(\omega)) + c\dot{z} + k_{eff}z = 0 \quad (14)$$

whose steady state solutions are (we are omitting the mode number from this point on as we only consider the first one):

$$z(t) = z_{drive,0}\delta z_0 e^{i\omega t + \varphi} \quad \text{with} \quad (15)$$

$$\delta z_0 = \frac{\hat{\omega}^2}{\sqrt{(1 - \hat{\omega}^2)^2 + 4\zeta^2\hat{\omega}^2}}; \quad \varphi = \arctan \frac{2\zeta\hat{\omega}}{1 - \hat{\omega}^2}; \quad \hat{\omega} = \frac{\omega}{\Omega}; \quad \zeta = \frac{c}{2m_{eff}\Omega}$$



**Figure 3:** Response of a damped resonator driven by an external vibration [1].

In Figure 3 we can see the response for different values of the *damping ratio*  $\zeta$ : we observe a lorentzian shaped peak in the amplitude and a  $+\pi$  phase shift in correspondence of the *resonance frequency*  $\omega_r$ , near the eigenfrequency of the system at:

$$\omega_r = \Omega\sqrt{1 - 2\zeta^2} \quad (16)$$

The maximum response, at resonance, is (for slight damping[1]):

$$\delta z_{max} = \delta z|_{\omega_r} = \frac{1 - 2\zeta^2}{2\zeta\sqrt{1 - \zeta^2}} \sim \frac{1}{2\zeta} \quad (17)$$

where the maximal amplification can be proven to be equal to the *quality factor*  $\mathcal{Q}$  [1].

The quality factor is defined as the ratio between energy stored in the system and energy lost in one oscillation:

$$\mathcal{Q} = 2\pi \frac{W}{\Delta W} \quad (18)$$

We can use the  $W$  and  $\Delta W$  [1] for a displacement  $z(t) = a\cos(\omega_r t)$  to prove that  $\mathcal{Q}$  is equivalent to the maximal amplification in (17):

$$W = \frac{1}{2}m_{eff}a^2\omega_r^2; \quad \Delta W = \pi c a^2 \omega_r \quad \longrightarrow \quad \mathcal{Q} = \frac{m_{eff}\omega_r}{c} = \frac{\sqrt{1 - 2\zeta^2}}{2\zeta} \sim \frac{1}{2\zeta} \quad (19)$$

The quality factor is also related to the sharpness of the resonance peak [1], with the -3dB bandwidth  $\Delta\omega_{-3dB}$  being related to it by:

$$Q = \frac{\omega_r}{\Delta\omega_{-3dB}} \quad (20)$$

The phase slope can also be expressed [1] in terms of  $Q$ :

$$\left. \frac{\partial\varphi}{\partial\omega} \right|_{\omega=\Omega} \sim \frac{2Q}{\Omega} \quad (21)$$

In our measurements we will use a small signal approximation of the phase response near the resonance to convert the phase measurement to a frequency signal, therefore an higher value of the phase slope, which is related to the quality factor by (21), results in a better frequency resolution.

### 1.3 Mass sensing and responsivity

The mass measurement is based on the shift in resonance frequency resulting from the mass variation in the oscillator. The *responsivity*  $\mathcal{R}_x$  of a sensor to a parameter  $x$  is defined as the slope of the sensor output  $y(x)$  vs. that parameter. We can work with a small signal approximation if the parameter variation is small enough, in which case the responsivity can be used to obtain the change in the parameter from the measured change in the output:

$$\Delta x \sim \frac{\Delta y}{\mathcal{R}_x} \quad (22)$$

The responsivity  $\mathcal{R}_{m_{eff}}$  to the effective mass for the simplified oscillator described in the previous section is given (for slight damping) [1] by:

$$\mathcal{R}_{m_{eff}} = \frac{\partial\Omega(m_{eff})}{\partial m_{eff}} \sim -\frac{\Omega(m_{eff})}{2m_{eff}} \quad (23)$$

In order to use it to measure the actual mass, we need to find the corresponding change in  $m_{eff}$ , that depends on the way the mass change is distributed. The responsivity can then be found from:

$$\mathcal{R}_m = \frac{\partial\Omega(m_{eff})}{\partial m_{eff}} \frac{\partial m_{eff}}{\partial m} \quad (24)$$

We will consider two situations: a distributed load along the length of the bridge and a point mass on a specific point.

**Distributed load** Adding a distributed load to the resonator, which in our case happens when filling the SMR with a liquid, has the same effect [1] as increasing the resonator's mass  $m_0$ , and we have:

$$\Delta m_{eff} = \frac{1}{2}\Delta m \quad \longrightarrow \quad \mathcal{R}_{m,distributed} \sim -\frac{\Omega(m_{eff})}{2m_{eff}} \frac{1}{2} = -\frac{\Omega(m_0/2)}{2m_0} \quad (25)$$

**Point mass** In the case of a point mass we have to actually consider its position  $x_{\Delta m}$ , as the effect on the effective mass depends on the value of the normalized mode shape in that point [1]. In our case (first bending mode) the dependence is:

$$\Delta m_{eff} = \phi_1^2(x_{\Delta m})\Delta m \quad \longrightarrow \quad \mathcal{R}_{m,pointmass} \sim -\frac{\Omega(m_{eff})}{2m_{eff}} \phi_1^2(x_{\Delta m}) \quad (26)$$

The maximum responsivity, for a mass at the center of the bridge, is:

$$\mathcal{R}_{max} \sim \frac{\Omega(m_0/2)}{m_0} \quad (27)$$



## 2 Suspended Microchannel Resonators

A *suspended microchannel resonator* (SMR) is a type of resonant mass sensor where the oscillator is a suspended microchannel and the samples to weight are transported through a microfluidic network [2, 3, 4]. The main advantages of using them over other solutions for mass sensing in liquids can be summarized with two main characteristics.

**Loss reduction** From (21) and (27) we know that in order to achieve an high resolution we need both an high quality factor and a low mass for our resonator.

If a resonator is immersed in fluid both of these parameters are degraded [3]: the viscous losses result in increased damping and therefore a worse quality factor, and the resonator has to move the surrounding liquid, resulting in an higher effective mass [1]. With an SMR, however, the fluid is confined *inside* of the resonator, which has been shown [2, 3] to almost eliminate high damping and viscous drag, with quality factors almost unchanged if compared to the dry resonator.

Quality factors up to 15000 have been demonstrated for SMRs, a significant improvement over conventional resonators in liquid, that only reach values up to  $\sim 150$  [3, 4].

**Integration with microfluidics** Another advantage of SMRs is the fact they can be integrated in a more complex microfluidic device [2, 3], which allows more complex control of the samples passing through the resonator. This leads to many possibilities, including:

- Controlling the sample speed during flow-through measurements, which is useful (as will be shown in the section describing the measurements) because it allows us to modulate the sensor's response duration to make it easier to distinguish from the noise;
- Regulating the concentration of particles or other solid samples that are transported through the SMR;
- Using a trapping system to stop the particles in the resonator [5, 4, 6], like the DEP trapping described in this work;
- Arraying multiple resonators to increase the measurement throughput [7].

### 3 Particle trapping with Dielectrophoresis (DEP)

Dielectrophoresis (DEP) is a phenomenon in which a non-uniform electric field can exert a force on a dielectric particle. DEP can be used in microfluidic systems to finely manipulate dielectric samples inside the channels in many ways, including moving them precisely, separating them by size or electric properties and stopping them by applying a force in the direction opposite to the fluid's flow.

#### 3.1 General working principle

When a particle is immersed in an electrolyte and subjected to an electric field, opposite sign charges will accumulate on both sides of the particle-medium interface, with more charges accumulating on the side with the higher polarizability [8].

This will generate an induced dipole in the particle along the field direction as the charge density is different on the two sides, and if the field is non-uniform the particle will be subjected [8] to a force

$$\mathbf{F} = (\mathbf{p} \cdot \nabla) \mathbf{E} \quad (28)$$

where  $\mathbf{p}$  is the dipole moment,  $\nabla$  is the del operator and  $\mathbf{E}$  is the electric field.

#### 3.2 DEP force

The DEP force acting on a particle can be obtained with one of two methods [8]:

- The *point-dipole method*, that approximates the particle as a point-charge dipole with the same potential;
- The *Maxwell stress tensor (MST) method*, that calculates the stress induced at the surface because of the electrical potential and integrates it over the particle surface to find the total force.

If we ignore higher order dipole moments and the particle is small compared to the spatial variation of the field both methods obtain the following force for a spherical particle [8]:

$$\mathbf{F}_{DEP} = 2\pi\epsilon_m f_{CM} R^3 \nabla |\mathbf{E}|^2 \quad \text{with} \quad f_{CM} = \frac{\epsilon_p - \epsilon_m}{\epsilon_p + 2\epsilon_m} \quad (29)$$

where  $\mathbf{E}$  is the electric field,  $\epsilon_m$ ,  $\epsilon_p$  are the absolute permittivities (respectively) of the medium and the particle. the liquid,  $R$  is the particle radius and  $f_{CM}$  is called the *Clausius-Mossotti (CM) factor*.

#### 3.3 DEP with an AC field

We now consider the case of an AC electric field, like the one used in this work for the particle trapping.

If we consider a stationary field with frequency  $\omega$ , we can represent it as:

$$\mathbf{E}(\mathbf{x}, t) = \Re \left\{ \hat{\mathbf{E}}(\mathbf{x}) e^{i\omega t} \right\} \quad (30)$$

For an AC field we have to consider the complex permittivities in the CM factor:

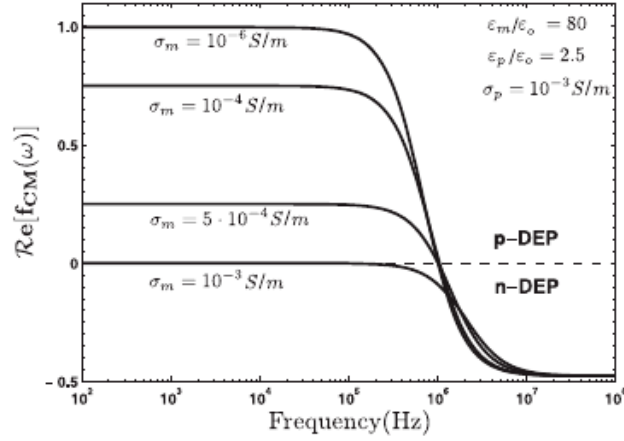
$$\tilde{\epsilon}_{m,p} = \epsilon_{m,p} - j \left( \frac{\sigma_{m,p}}{\omega} \right) \quad \longrightarrow \quad f_{CM}(\tilde{\epsilon}_m, \tilde{\epsilon}_p) = \frac{\tilde{\epsilon}_p - \tilde{\epsilon}_m}{\tilde{\epsilon}_p + 2\tilde{\epsilon}_m} = \frac{(\epsilon_p - \epsilon_m) + j(\sigma_p - \sigma_m)/\omega}{(\epsilon_p + 2\epsilon_m) + j(\sigma_p + 2\sigma_m)/\omega} \quad (31)$$

The resulting average force on a spherical particle can be expressed [8] as:

$$\langle \mathbf{F}_{DEP}(t) \rangle = 2\pi\epsilon_m \Re \{ f_{CM} \} R^3 \nabla \mathbf{E}_{rms}^2 \quad (32)$$

where  $E_{rms}$  is the root-mean-square of the applied field's amplitude.

We can extract the main features of the DEP force from (32) [8]:



**Figure 4:** Example of a typical behaviour for the CM factor, relative to polystyrene particles suspended in various aqueous solutions [8].

- The average DEP force depends on  $\nabla \mathbf{E}_{rms}^2$ , meaning that the direction, polarity and absolute amplitude of the field have no effect on the DEP force, just its variation in space;
- The sign and magnitude of the force depend on the term  $\epsilon_m \Re\{f_{CM}\}$ , which introduces a dependence on the electrical properties of the particle and medium. If  $\Re\{f_{CM}\} > 0$  (*pDEP*), the particle will be attracted by the field maxima and repelled from the minima, if  $\Re\{f_{CM}\} < 0$  (*nDEP*) the opposite happens.
- While the medium and particle are not generally free to choose, we can tune the CM factor by changing the frequency of the DEP field: the sign and magnitude of the CM factor (and therefore of the DEP force) are mostly determined by the electrical conductivities at low frequencies, while the permittivities dominate at high frequencies (Fig. 4). This can allow for tunable selective manipulation of particles with different electrical properties.
- The force is proportional to the particle volume, meaning that it is possible to manipulate particles in different ways depending on their size;

### 3.4 DEP trapping in the SMR device

The device described in this work uses two planar electrodes above the bridge to create a strong field region between them, extending inside the resonator. The spatial variation of the field is strongest at the borders of this zone, meaning that depending on the sign of the CM factor the stopping region is near the edge of one of the electrodes: *pDEP* stops particles as they leave the high-field region, *nDEP* stops particles trying to enter it.

Both the stopping region's size and the maximum force that the DEP can apply depend on how sharply the field increases at the border of the high field region, which is influenced by the shape and electrical properties of the electrodes and bridge.

If all forces acting on the particle except the drag force and the DEP force can be neglected, the particle speed along the channel direction is governed by [8]:

$$m_p \dot{v} = 6\pi\mu R(v_m - v) + 2\pi\epsilon_m \Re\{f_{CM}\} R^3 \partial_x (\mathbf{E}_{rms}^2) \quad (33)$$

where  $v_m$  and  $v$  are the fluid and particle velocities along the x direction and  $m_p$  is the particle mass.

If the deceleration time is much smaller than the scale of the field variation, then we can ignore the acceleration term in (33) and set  $v < 0$  to find the values of  $\partial_x (\mathbf{E}_{rms}^2)$  that stop or push back the

particle:

$$\partial_x(\mathbf{E}_{rms}^2) > \frac{3\mu v_m}{\epsilon_m R^2 \Re\{f_{CM}\}} \quad (34)$$

### 3.5 Comparison with other trapping approaches for SMR

In literature various techniques have been demonstrated to slow down or stop samples inside a microfluidic channel, but many of these methods require complex structures or surface functionalization within the channel.

**Mechanical traps in the SMR** By adding internal structures in the SMR that block the passage of the samples but not the flow of liquids (similarly to a fishing net), the former can be trapped inside a section of the SMR and kept there during the measurement [5].

This approach can trap the samples very stably and introduce different liquids during the measurements while monitoring the mass changes, and is therefore good for biological measurements, but requires complex fabrication for the trapping structures and samples have an higher risk of getting stuck on the walls of the SMR if compared to DEP trapping.

**Acoustic trapping** By using an array of ultrasonic transducers, this technique creates an acoustic standing wave in a microfluidic channel, that can be used to manipulate particles in a noncontact way [9, 10]. This method has a similar effect to DEP without the need to polarize the samples, but the integration of the transducers is significantly more complex with respect to the DEP electrodes.

**Chemical trapping on a surface** The inner surface of the channel can be functionalized to selectively adsorb specific molecules [10]. This can be used to achieve high selectivity and precise control of the sample position during the measurement, but does not work with all samples and usually requires a dedicated mechanism to reverse the attachment.

## 4 Device specifics and fabrication process

### 4.1 Design choices

The SMR-DEP device that is the subject of this work inherits most of its design and fabrication requirements from the monolithic glass SMR devices [11, 12] it is based on, with the main difference being the integration of two coplanar electrodes for dielectrophoretic trapping.

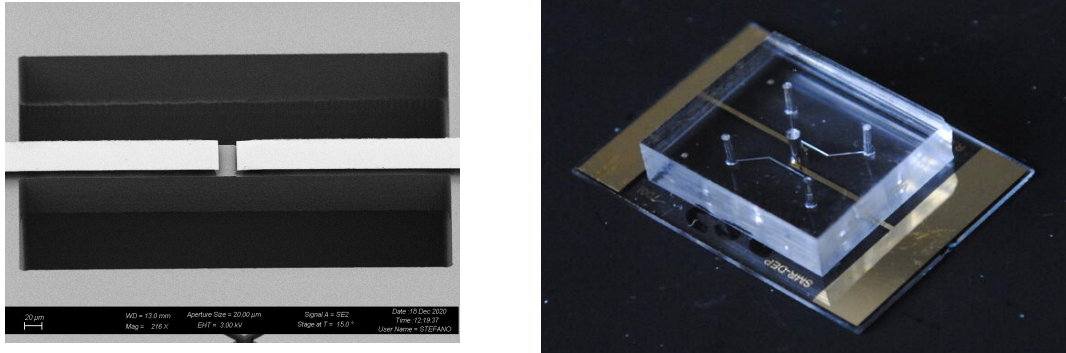
#### 4.1.1 Suspended bridge

The resonating bridge is a crucially important element in designing this SMR, as the performance of the sensor is ultimately dependent on it.

A doubly clamped beam design was chosen for the resonator, as the integration of the DEP electrodes is easier if compared to the case of a single clamped resonator with an U-shaped channel [13].

The mass, size (in particular the aspect ratio  $L/h$ ) and mechanical properties of the bridge are the main factors in determining its mass responsivity [1], and the frequency noise is also mostly dependent on the resonator intrinsic damping [3] and therefore on its mechanical properties. The roughness of the SMR's surfaces is also a factor as it affects the laser's reflection and the passage of fluids inside the channel.

The dimensions of the device were optimized to achieve the highest possible responsivity within the process constraints.



**Figure 5:** *Left: SEM image of one of the 250μm long SMR bridges; Right: photo of the complete device showing the electrodes, the microfluidic channels and the PDMS interface.*

The femtosecond laser process spot size (with 50x objective) imposes a minimum diameter of  $10\mu\text{m}$  for the channel and (along with the minimum step between the laser spots) a minimum thickness of  $30\mu\text{m}$  for the entire beam [11]; these constraints force a nominal height of  $30\mu\text{m}$  for the beam and of  $15\mu\text{m}$  for the channel if we want to minimize the resonator mass while having enough space for particles to pass.

The ratios between the beam dimensions have been optimized to separate in frequency in-plane and out-of-plane modes [11, 12], and the width of the channel relative to the width of the beam has been chosen to maximize the liquid to solid ratio, which is linked to device performance [11]. The widths chosen (nominal values) for our device are  $75\mu\text{m}$  for the beam and  $55\mu\text{m}$  for the channel, and two different lengths of  $250\mu\text{m}$  and  $500\mu\text{m}$  were selected for this device.

#### 4.1.2 Microfluidics

Most of the microfluidics connections are machined directly on the chip, with a  $1.93\text{mm}$  long buried central channel passing through the bridge and connecting to 2 bypass channels (square section  $25\mu\text{m} \times 25\mu\text{m}$ ) sealed with a PDMS interface with 4 microfluidic inlets. For this reason, the bypass channels are exposed on one side instead of being buried like the central one. Each of the 4 channels branching out from the central channel include a serpentine to slow down passing samples, reaching a total length of  $22.4\text{mm}$  for each branch. This design enables an higher degree of control over the fluid and sample transport, which makes the device operation more convenient.

The device is bonded to the PDMS cover including 5 holes, 4 being circular inlets compatible with standard microfluidics tubing and one to keep the area above the bridge free.

#### 4.1.3 Electrodes for DEP

The coplanar electrodes are patterned out of 4 metal layers, from the substrate the order is Cr/Au/Cr/Au. The chromium layers are  $20\text{nm}$  thick and the gold layers are  $200\text{nm}$  thick.

The electrode configurations used in literature for DEP trapping generally contact the liquid [8], but here the electrodes are on top of the bridge. They are patterned to have two contacts along the side of the chip, a section extending to the central channel and then a final one above it and the bridge, with a  $20\mu\text{m}$  gap between them, positioned  $10\mu\text{m}$  off-center: the electrodes are designed to create a strong electric field under the gap, which ideally results in the DEP stopping zone being at the center of the resonator, where the sensitivity is highest.

The strong field in the part of the channel between the electrodes will stop a certain fraction of the samples that pass through the channel, depending on size, density, speed and dielectric constant [6].

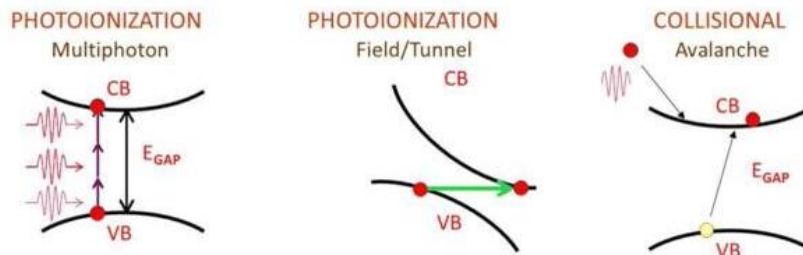
### 4.2 Fabrication process

The device fabrication process is kept relatively simple, with a limited number of processing steps, thanks to the combination of two main factors: the use of femtosecond laser direct writing to fabricate the resonating bridge and the buried microfluidic channels in a single step, and the choice to have the DEP electrodes all on one side of the chip.

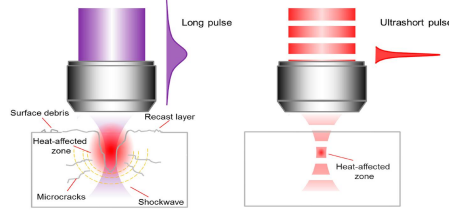
#### 4.2.1 Femtosecond laser machining of transparent materials

Femtosecond laser micromachining is a technique that can be used to perform 3D-resolved machining of complex structures in transparent materials with a two-step process (ablation+selective etching) based on non-linear optical absorption of femtosecond laser pulses.

The process only major limitations are the need to use a dielectric material that is transparent to the laser's wavelength and the minimum size of the focal point.



**Figure 6:** *Nonlinear ionization processes*



**Figure 7:** *Effect of laser pulse duration.*

**Nonlinear absorption processes** By definition, a transparent material has energy gap  $E_g$  greater than the laser photon energy  $h\nu$ , therefore there is no linear absorption and non-linear phenomena requiring high intensities to take place at a relevant rate are the only absorption mechanisms available.

Three main ionization processes are involved in femtosecond laser writing [14]: multiphoton absorption, tunneling and avalanche.

Multiphoton ionization consists in the simultaneous absorption of  $n$  photons  $h\nu$ , where  $n$  is such that  $nh\nu > E_g$ .

Tunnelling ionization occurs when the laser pulse's electrical field is temporarily high enough to overcome the energy gap and enable tunneling from the valence band to the conduction band.

Avalanche ionization involves conduction band electrons acquiring kinetic energy through multiple photon absorptions until their energy is sufficient to promote a valence band electron to the conduction band, resulting in two electrons at the  $E_C$  that can be ionized again; the free electron grows exponentially for as long as the field accelerates the electrons.

**Pulse duration effect** For long ( $> 1ps$ ) pulses, the intensity isn't high enough for relevant multiphoton or tunneling ionization, and the main ionization process is avalanche starting from a limited, highly variable number of "seed" electrons, mostly generated from defect states in the gap, resulting in a very high variability.

Shorter ( $< 1ps$ ), more intense pulses are sufficient to enable tunneling and multiphoton ionization mechanisms, resulting in a much more controllable number of electrons promoted to the conduction band, that can then act as *seeds* for avalanche ionization, resulting in a controlled and reproducible deposition of energy that does not have the time to transfer to the lattice in the short pulse time.

**3D-resolved material modification** If the deposited energy surpasses a certain threshold, the material undergoes permanent modification, whose nature depends on material and exposure.

By tightly focusing the laser and adjusting the laser fluency and/or pulse duration the affected zone can be reduced to a small focal volume, resulting in 3D-resolved material modification: this is the reason why femtosecond laser pulses are ideal for our purposes.

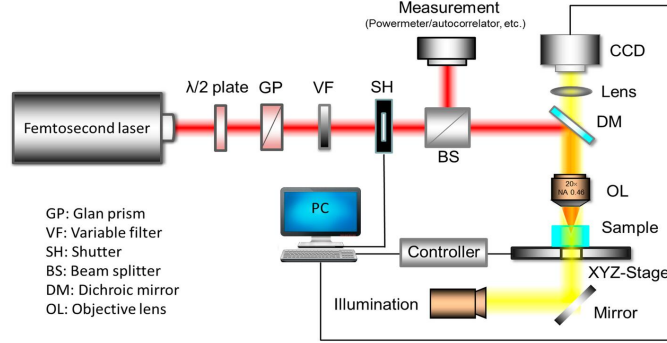
**Laser-assisted etching of silica** In the case of silica, the modification induced by the femtosecond laser is a decrease of the glass's chemical resistance against certain etchants.

The exact mechanism is not yet clear, but two possible mechanisms could explain the effect: stress induced by the irradiation changing the Si-O-Si bond angle, and the formation of nanocracks with a consequent increase of the effective surface for the etching reaction [11].

Both HF and KOH can be used for the etching step, the latter was chosen in our case: despite the lower etching rate it exhibits an higher selectivity for the modified areas ( $\sim 200$ ) which remains stable during the long processes needed for high aspect ratio structures and no length saturation (a reduction of the acid permeability that can occur high aspect ratio structures) [11].

The main drawback of the process is it leaves a rougher surface than standard micromachining techniques, up to hundreds of nanometers, that can however be mitigated by post-processing steps

[11] like annealing the device to reflow the glass. In our case this was not possible as the heat would melt the electrodes.



**Figure 8:** *Femtosecond laser direct writing setup.*

**Laser direct writing system** The 3D printing system (Fig. 8) used to make the SMR chip's bridge and channels includes[11]:

- A  $\lambda = 1030nm$  Ytterbium laser;
- A series of optical elements used to control the laser power and a mechanical shutter used to control the pulse duration;
- An interferometric setup used to monitor the input laser stability;
- A 50x objective ( $NA = 0.65$ ) used to focus the beam;
- A control system for the shutter and stage;
- An high-precision XYZ scanning stage for the sample;
- An illumination+CCD camera setup used to monitor the writing procedure.




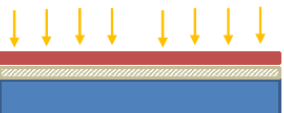



#### 4.2.2 Fabrication process of the SMR-DEP device

**Electrode deposition and patterning** The electrodes for the DEP are the first element added to the chip; the process steps are reported in Table 1, and Figure 9 shows the patterned electrodes.

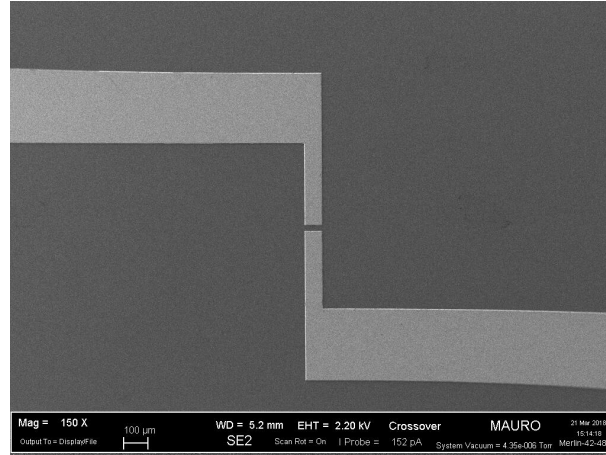
**Suspended structure and embedded channels** The femtoprint [15] fabrication process (Fig. 10) was used to make the suspended resonator and the microfluidic channels. As said before, this process is relatively simple, with only a few steps.

1. The femtosecond direct writing process is used to directly expose the parts of the glass substrate that need to be removed: the writing is done in a rasterized way, with the scanning system used to sequentially expose adjacent "dots". The exposure is performed from the opposite side of the device to avoid damaging the electrodes. The entire channel network (including the buried central channel) and the gap around the bridge are exposed;
2. High-T KOH wet etching is used to selectively remove the exposed sections [11];
3. The chip is rinsed in deionized water and dried [15].



Step	Description	Cross-section
1	The wafer is chemically cleaned with Piranha solution ( $H_2SO_4 + H_2O_2$ );	
2	The metal layers for the electrodes ( $Cr20nm/Au200nm/Cr20nm/Au200nm$ ) are sputtered on top of the wafer, the high temperature process increases the electrodes' etching resistance;	
3	A $2\mu m$ layer of positive photoresist (PR) is deposited on the wafer;	
4	The PR is exposed with direct writing photolithography;	
5	The PR is developed and a reflow step is performed;	
6	Ion beam etching is used to pattern the electrodes;	
7	The PR is stripped away in two steps (plasma+wet etchant).	

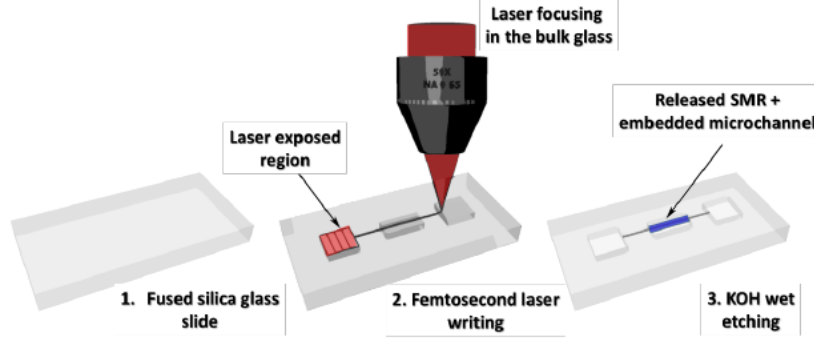
**Table 1:** Process steps for the electrodes' fabrication.



**Figure 9:** SEM image of the patterned electrodes.

**PDMS interface fabrication and bonding** To enable connection with external microfluidics and to seal the on-chip channels the device (Fig. 11, left) is bonded to a PDMS cover.

First, a mold (Fig. 11, right) for the PDMS cover is fabricated with standard silicon patterning techniques [11], as shown in Table 2.



**Figure 10:** Summary of the femtoprint process relative to the non-DEP device: the process has not changed since.

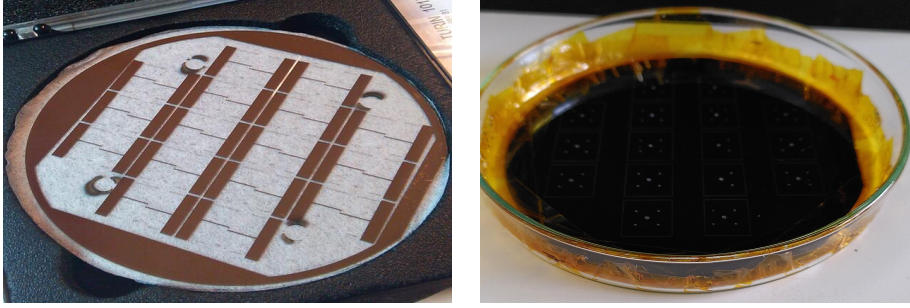
Step	Description	Cross-section
1	The silicon wafer is coated with PR;	
2	The PR is exposed with the mold's inverted pattern via laser direct writing;	
3	The PR is developed;	
4	The pattern is transferred to the substrate with Deep Reactive Ion Etching (DRIE);	
5	The resist is stripped;	
6	The surface of the mold is silanized to passivate the surface and prevent sticking.	

**Table 2:** Process steps for the PDMS mold fabrication.

Step	Description	Cross-section
1	PDMS with 10:1 co-polymer/cross linker ratio is poured on top of the mold in a $\sim 5mm$ thick layer;	
2	The PDMS is cured and the PDMS interfaces are demolded and separated.	

**Table 3:** Process steps for the PDMS interface fabrication from the mold.

The mold can then be used to prepare the PDMS interfaces[11], as explained in Table 3.



**Figure 11:** *Left: SMR-DEP chips before bonding; Right: Mold for the PDMS interfaces.*

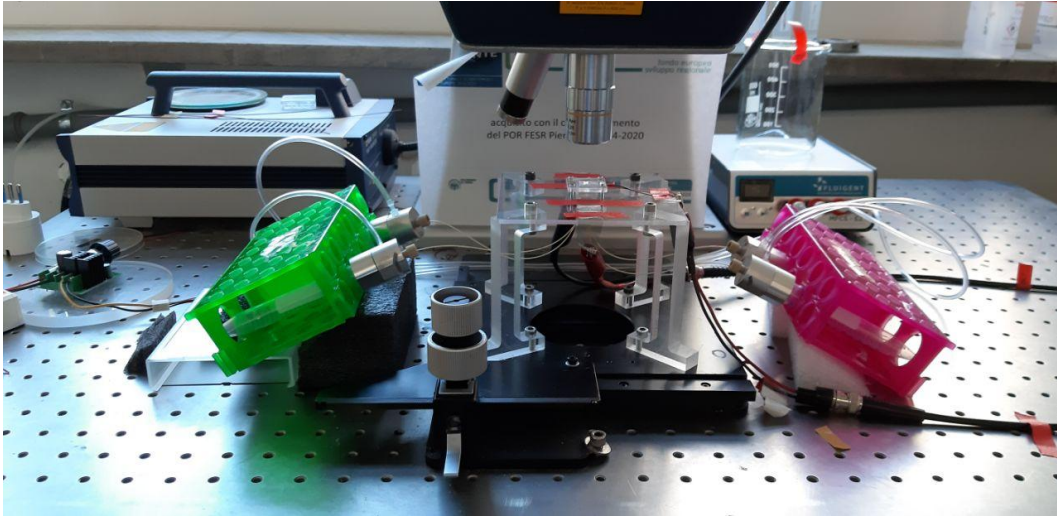
Finally, the interfaces are bonded to the SMR-DEP chips [11].

1. First, the PDMS and chip surfaces that are to be bonded are activated with oxygen plasma. The process parameters are optimized to maximize the bonding strength;
2. The PDMS is pressed onto the chip immediately after the activation to bond the two together.

## 5 Measurement set-up

In order to perform the measurements, our setup (shown in Fig.12) needs to have the following elements:

- An holder to keep the device in position, that needs to filter out as much external vibration as possible, combined with a scanning system capable of precise movement along the horizontal directions;
- A microfluidics setup to control the flow of liquids through the device;
- An actuation method to excite the oscillator;
- A read-out setup to measure the oscillator response and decouple it from the actuation;
- A control+driving system to control the DEP and actuation.



**Figure 12:** *Measurement setup for the SMR-DEP device.*

### 5.1 Sample positioning and isolation from vibrations

To reduce the influence of external vibrations, the holder with the device and the microfluidics system are positioned on an antivibration table.

The table is fitted with a precise positioning system, consisting in a metal plate that can be moved precisely along two rails (in the X and Y direction respectively) using two knobs; the plate has screw holes used to fasten the sample holder's legs to it.

The sample holder itself consists in a plastic pane with a central hole for the fluidic inputs, bolted to 4 legs used to leave enough space below the pane for the fluidics tubing and the wires going to the DEP and actuation electrodes. The chip is held over the hole by two PDMS supports, and kept firm by a plastic part with holes for the optical readout and the actuation, that goes above the chip and is screwed to the holder.

### 5.2 Microfluidics setup

The microfluidic setup consists in 4 vials acting as reservoirs, fitted with valves each connected to 2 tubes; one of the tubes is connected to a Fluigent MFCS-EZ microfluidic controller and is used to

regulate (with compressed air) the pressure that drives liquid into the second tube, that connects to the device's inlets through metal connectors.

Two vial holders each contain two of the vials and are kept on the sides of the sample holder with polystyrene supports.

As the solution with the particles used in the measurements is usually in the top-left vial, a magnetic stirrer is fitted underneath the left vial holder.

### 5.3 Actuation method and read-out system

The device uses an external piezoelectric actuator, fixed on top of the chip with biadhesive tape. Conductive wires soldered to the contacts can be used to drive the actuator; in our case the actuator is driven by the Zurich HF2LI lock-in amplifier's output (see the relevant section below).

The read-out is optical: a Polytec OFV-551 laser Doppler vibrometer is used to measure the speed of the oscillator along the laser's direction.

In short, a Doppler vibrometer uses an interferometric setup to measure the frequency shift that a laser undergoes when it is reflected from a moving sample's surface, which using the Doppler effect is used to obtain the sample's velocity with  $\Delta\nu_{Doppler} = 2\frac{v}{\lambda}$ , where  $\lambda$  is the laser's wavelength. The vibrometer's control decodes the interference signal, generating a signal proportional to the velocity of the sample (that can be integrated to obtain the displacement).

### 5.4 Signal processing and control system

A lock-in amplifier is used to drive the actuator and demodulate the vibrometer response. The demodulator uses a mixer to multiply the signal with a reference (in our case the actuator's driving signal), then applies a low pass filter to the result; this has the effect of filtering all signal components that are not at the reference frequency, obtaining a signal whose amplitude and phase correspond to the device's response at that frequency.

By doing a sweep with the input frequency, we can obtain the complete spectrum of the amplitude and phase response in the sweep interval, this will be referred to as a "sweep" in the following sections.

By actuating at a constant resonance frequency, corresponding to a peak in the spectrum, and monitoring the phase of the response, we can detect shifts in it, that can be converted into frequency shifts with the help of the phase of the device response measured from a sweep measurement. We will call this an "open loop" measurement, as opposed to a "closed loop" measurement that changes the actuation frequency to keep the phase constant and monitors said change.

### 5.5 DEP setup

The DEP electrodes on the chip are contacted by strips of metal mesh tape that allow for easier driving of the DEP field; the strips are kept firm between the chip and the PDMS supports and further fastened with adhesive tape.

High voltages are needed to obtain a strong enough DEP field, so an RF amplifier is coupled to the wave generator used to drive the DEP voltage.

## 6 Device characterization and measurements

Two sets of preliminary measurements, without any particles, were performed to characterize the mechanical response of the devices and the Allan noise associated with them.

Four sets of devices were used:

- Prototypes fabricated without any electrodes, identified by a lowercase letter ("a" for the  $250\mu m$  long devices and "b" for the  $500\mu m$  long ones). These devices will also be referred to, respectively, as the "SMR-250" and "SMR-500" devices;
- Finished devices with the DEP electrodes on them, identified by an uppercase letter ("A" for the  $250\mu m$  long devices and "B" for the  $500\mu m$  long ones) and a serial number. We will refer to these devices as the "SMR-DEP-250" and "SMR-DEP-500" devices.

### 6.1 Resonance spectra - Air

Two sets of sweep measurements were performed on the empty devices to obtain the resonance spectra: one on the new devices and a second one after a few weeks of operation. Both sets are shown in Figure 13, comparing the spectra belonging to each set of devices.

**Results and observations** The bridge is quite far from the ideal double-clamped beam: it is hollow, its form factor is relatively low ( $\sim 8.2$  for the short bridges and  $\sim 16.4$  for the long ones, with a value greater than 10 being considered ideal [1]) and the surface is left quite rough from the fabrication process. Moreover, for the SMR-DEP devices the process leaves an overetched zone underneath the electrodes, making it easier for parts of them to break off and leaving them partially suspended near the edges. All of these things can explain wider peaks with more complex shapes if compared to the single sharp peak predicted [1] for an ideal oscillating bridge.

By monitoring the bridge during measurements we realized that, across the space of multiple measurements, some of the electrodes had become slightly but noticeably smaller, with pieces breaking off from areas suspended because of overetching. Shifts towards higher frequencies observed between the older and newer measurements are likely linked to this phenomenon.

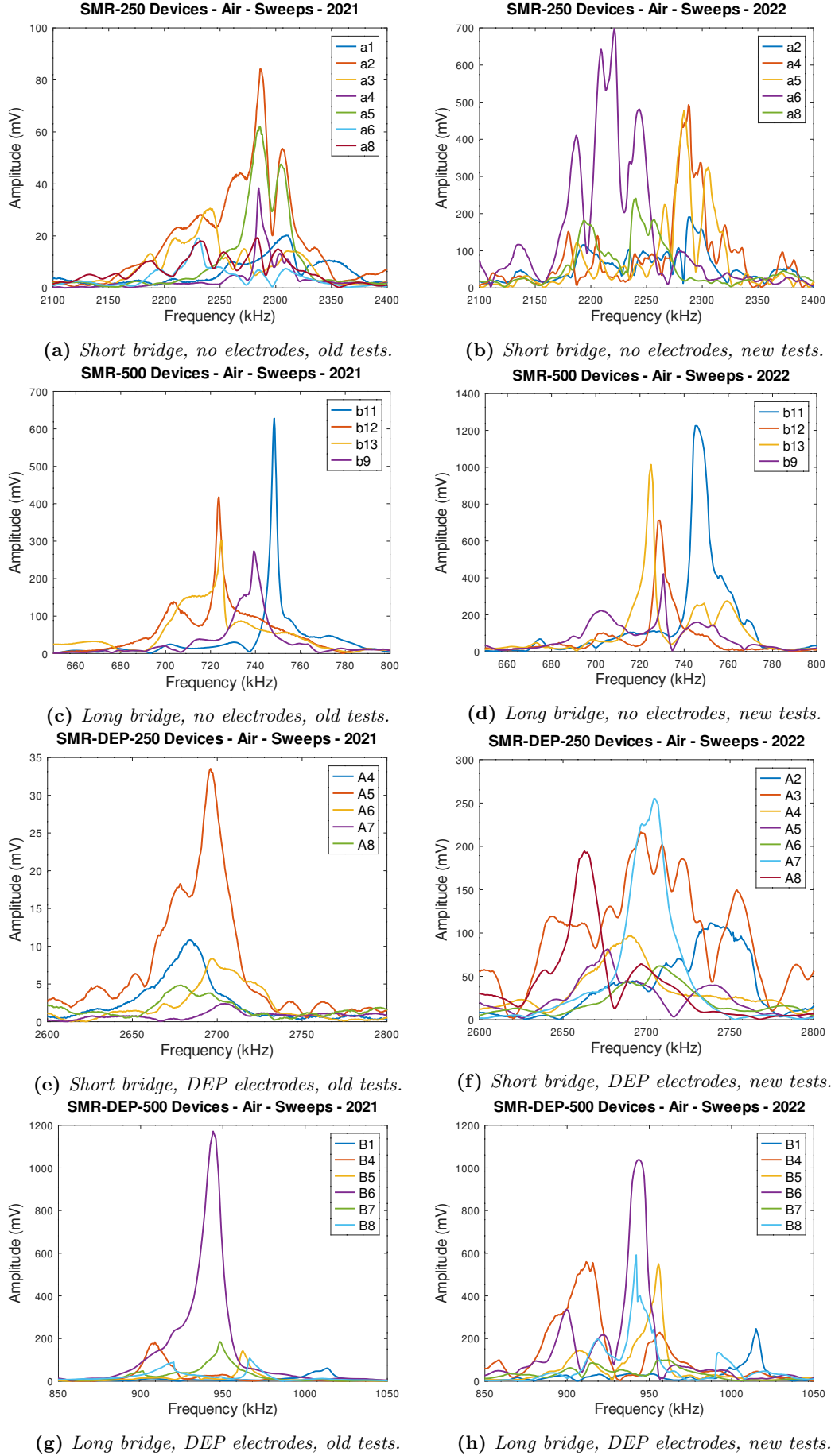
### 6.2 Resonance spectra - Liquids

By performing sweeps with different liquids inside the resonator and evaluating the shift of the resonance peaks we can estimate the devices' responsivities  $\mathcal{R} = \Delta\nu_{res}/\Delta m$  and their masses, and compare them with the theoretical predictions.

In order to measure these shifts, we completed many sweep measurements in air and using solutions with different combinations of water and ethanol (the same measurements are also used as reference in post-processing the flow-through particle measurements, described in a later section); here we show a subset of them following these criteria:

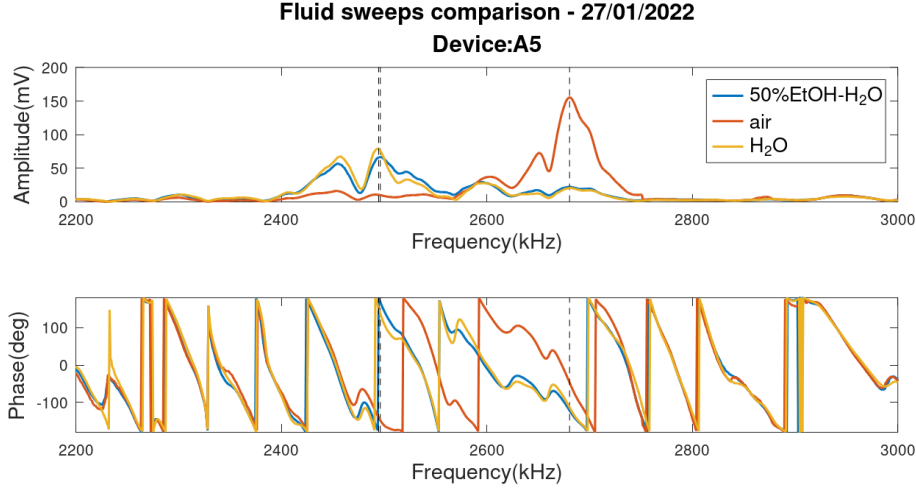
- All measurements were performed on devices from the SMR-DEP-250 set, featuring both the complete configuration with DEP electrodes and a shorter bridge, capable of higher responsivity;
- The measurements are grouped in sets, performed within a limited time span (consecutive days if not a single one) on the same device filled with different fluids.

**Example process** In Figure 14 we show and compare the sweep results for one of the datasets (A5 device, taken on 27/1/22) as an example of the comparison process used and of the difficulties encountered. The shape of the spectrum changes depending on the fluid inside the resonator, so



**Figure 13:** Comparison of the resonance spectra for the empty devices.





**Figure 14:** Example comparison of sweeps with different liquids, the vertical lines highlight the resonance peaks chosen.

identifying the bridge resonance in each condition is not trivial if we look at the amplitude, but the phase offers a more reliable way to do it.

For two sweeps with different fluids in the resonator, a difference in phase can be observed in the area between the respective resonance peaks, which can be used to distinguish them from peaks that didn't shift.

**Results and Observations** In Figure 15 we plot the resonance frequencies against the liquid mass in the resonator (which we have obtained from the nominal values of the bridge cavity volume and liquid densities) and do a linear fit for each dataset to obtain an estimate of the resonator's responsivity  $\mathcal{R}$  (as the fit's slope) and of its mass  $m_{air}$  when filled with air; both values are reported in Table 4 along with the measured resonances.

In the plots in Figure 15 we observe values in the  $2670\text{kHz}$  to  $2730\text{kHz}$  range for the resonance in air, from which assuming the mass of  $1267\text{ng}$  (obtained from the nominal sizes and density of the resonator) we could theoretically[1] expect (from  $\mathcal{R}_{theory} \equiv \mathcal{S} = -\nu_{air}/(2 * m_{air})$ ) values of responsivity within the  $-1.0774(\text{kHz/ng})$  to  $-1.0536(\text{kHz/ng})$  interval.

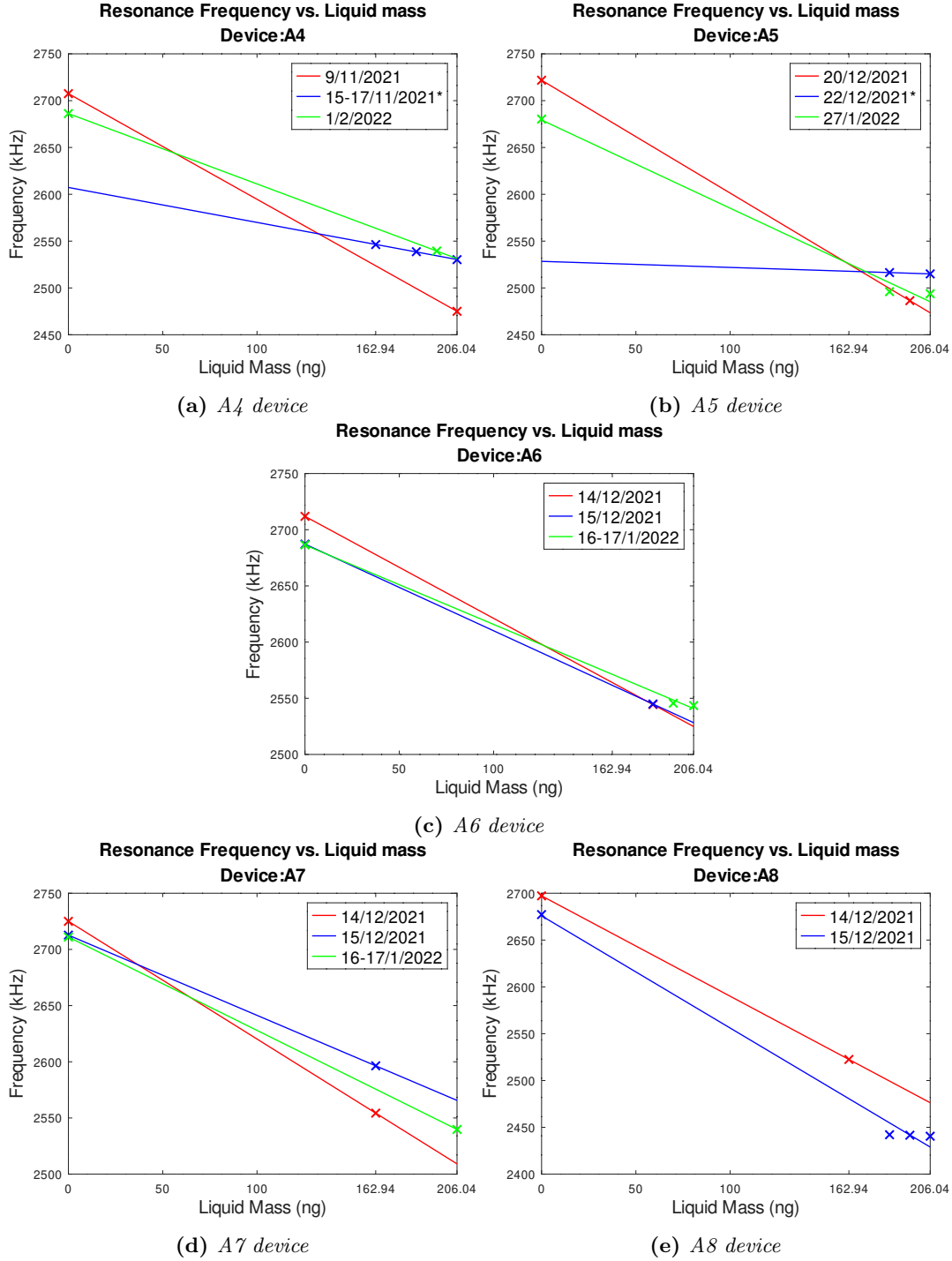
In reality, we can see from the data in Table 4 that the responsivities obtained from the fit slopes have a wider range (from  $-1.2055\text{kHz/ng}$  to  $-0.7082\text{kHz/ng}$ ), as do the corresponding values of  $m_{air}$ , which are in the  $1116\text{ng} \div 1900\text{ng}$  range. This range excludes the datasets without a measurement in air (marked with \* in Table 4), as the linear fit results for those give completely unrealistic values, as we can observe from Table 4. This inconsistency reflects the fact that the resonance shifts between measurements done in liquid (within each dataset) are significantly smaller than the theory would predict; this behaviour could be attributed to:

- Systematic error occurring during the solutions' preparation or an unknown process altering the concentrations;
- Some other contribution other than the mass altering the positions of the peaks, like coupling between the bridge resonance and another oscillation of the device causing a splitting of the peaks;
- Environmental factors such as temperature or pressure changing between the measurements and affecting the results.



Device	Date	Loading	Resonance(kHz)	$m_{air}(ng)$	$\mathcal{R}(kHz/ng)$	$\mathcal{S}(kHz/ng)$
A4	9/11/21	<i>Air</i>	2707.5	1199.71	-1.1284	-1.0685
		$H_2O$	2475.0			
	16/11/21	<i>EtOH</i>	2546.3	3245.80*	-0.3735*	-
	17/11/21	$50EtOH - H_2O$	2538.7			
	15/11/21	$H_2O$	2530.2			
	1/2/22	<i>Air</i>	2686.2	1786.54	-0.7518	-1.0601
		$25EtOH - H_2O$	2539.4			
A5	20/12/21	<i>Air</i>	2721.8	1128.88	-1.2055	-1.0741
		$25EtOH - H_2O$	2486.4			
	22/12/21	$50EtOH - H_2O$	2516.4	19185.60*	-0.06496*	-
		$H_2O$	2515.0			
	27/1/22	<i>Air</i>	2680.3	1341.54	-0.9990	-1.0577
		$50EtOH - H_2O$	2496.0			
		$H_2O$	2493.8			
A6	14/12/21	<i>Air</i>	2711.9	1493.49	-0.9080	-1.0702
		$50EtOH - H_2O$	2544.4			
	15/12/21	<i>Air</i>	2687.2	1741.96	-0.7713	-1.0605
		$50EtOH - H_2O$	2544.9			
	16/12/21	<i>Air</i>	2686.5	1896.69	-0.7082	-1.0602
		$25EtOH - H_2O$	2545.6			
A7	19/10/21	<i>Air</i>	2725.0	1300.54	-1.0476	-1.0754
		<i>EtOH</i>	2554.3			
	4/11/21	<i>Air</i>	2712.7	1900.26	-0.7138	-1.0705
		<i>EtOH</i>	2596.4			
	8/11/21	<i>Air</i>	2711.0	1631.38	-0.8309	-1.0699
		$H_2O$	2539.8			
A8	18/10/21	<i>Air</i>	2697.2	1257.80	-1.0722	-1.0644
		<i>EtOH</i>	2522.5			
	7/2/22	<i>Air</i>	2677.2	1116.95	-1.1984	-1.0565
		$50EtOH - H_2O$	2442.1			
		$25EtOH - H_2O$	2441.6			
		$H_2O$	2440.5			

**Table 4:** Results and fit parameters for the sweeps with liquids. The fit results marked with \* were obtained without an air measurement and are only shown for completeness as they offer completely unrealistic estimates.



**Figure 15:** Resonance frequencies vs liquid mass in the bridge, fitted by dataset. The datasets marked with \* don't have an air measurement and their fit produces unrealistic results.

### 6.3 Allan Deviation

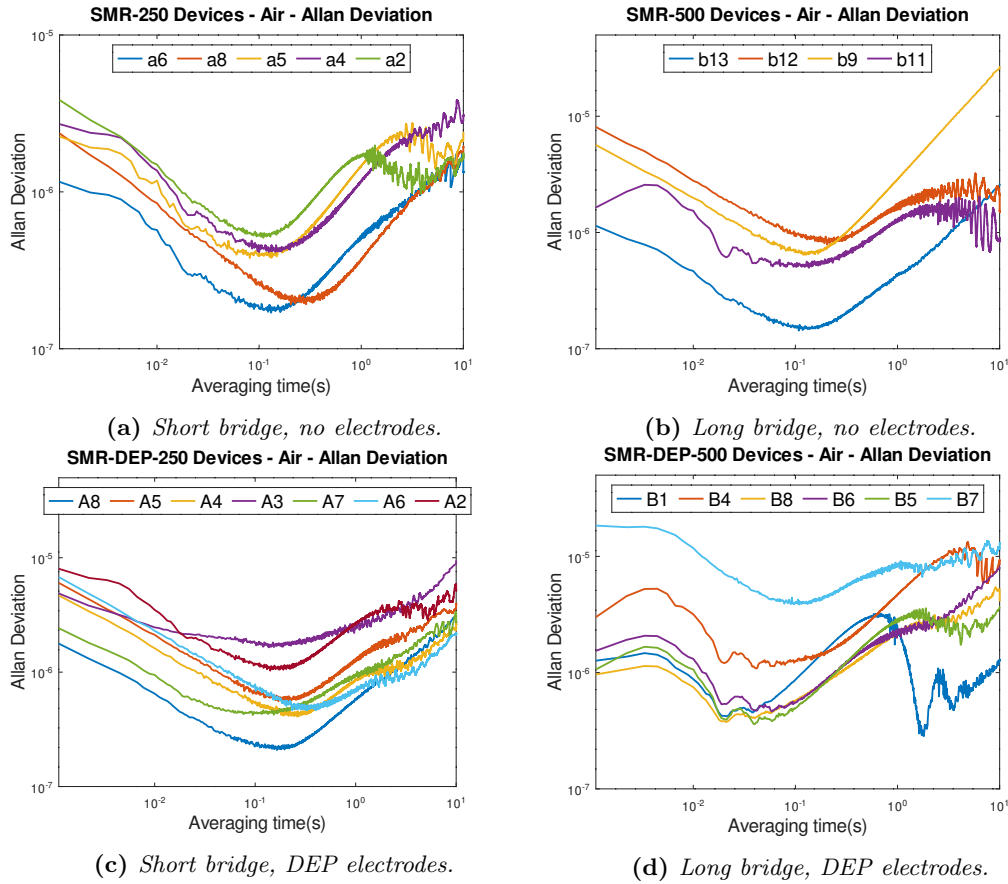
We can now proceed to the characterization of the Allan deviation  $\sigma_{Allan}(\tau)$  for the empty devices, which is defined as the average of the squared differences between successive samples of a measured quantity, taken with an interval  $\tau$ .

The Allan deviation for  $\tau = n\tau_0$ , where  $\tau_0$  is the measurement interval, is obtained by averaging the samples in blocks of  $n$  and using those as samples. For this to be valid,  $\tau$  must be lower than  $T/2$ , where  $T$  is the total measurement time.

The minimum value of the Allan deviation gives us an idea of the stability of our measurements, while the slope of the log-log plot gives us informations on the type of noise. For each device, after taking sweeps to find the resonance frequencies, we performed open loop measurement at those frequencies, making sure to use a bandwidth more than double the sampling rate ( $2kHz$  for a sampling rate of about  $900Hz$ ) to avoid losing any information. The open loop measurements were converted from a phase value to the corresponding frequency value inverting the phase response of the sweeps (which we approximated as linear in a neighbourhood of the resonance).

After that we computed the Allan deviations (square root of the variance), which are shown in fig. 16. These measurements were part of the more recent set of mechanical characterization tests, and were taken in the same conditions as the second set of sweeps in the previous section.

**Results and observations** Table 5 summarizes the minimum values  $\sigma_{Allan,min}$  for the Allan deviation in air and its values for an averaging time  $\tau$  of 100ms (which is near to a typical passage time for particle measurements) for each device along with the operation frequency  $\nu_0$  for the measurement.



**Figure 16:** Comparison of the Allan deviations in air vs. averaging times (log-log plots).

Device	Device set	Frequency(kHz)	$\sigma_{Allan,min} (10^{-7})$	$\sigma_{Allan} \tau=100ms (10^{-7})$
a2	SMR-250	2288.4	5.0989	5.2723
a4	SMR-250	2287.8	4.1307	4.1551
a5	SMR-250	2283.4	3.7821	4.0945
a6	SMR-250	2221.3	1.6959	1.8055
a8	SMR-250	2239.2	1.9180	2.6001
b9	SMR-500	730.5	6.4158	7.0922
b11	SMR-500	745.6	4.9666	5.1146
b12	SMR-500	728.7	7.8495	9.8787
b13	SMR-500	724.8	1.4324	1.5320
A2 <sup>†</sup>	SMR-DEP-250	2738.9	10.295	11.844
A3 <sup>†</sup>	SMR-DEP-250	2697.7	16.462	18.114
A4	SMR-DEP-250	2690.1	4.0886	5.4946
A5	SMR-DEP-250	2676.6	5.5099	6.5287
A6	SMR-DEP-250	2708.0	4.6284	7.8101
A7 <sup>†</sup>	SMR-DEP-250	2704.9	4.2148	4.3791
A8	SMR-DEP-250	2663.2	2.0828	2.3194
B1	SMR-DEP-500	1014.8	4.2119	8.7037
B4	SMR-DEP-500	911.7	10.844	12.437
B5	SMR-DEP-500	955.4	3.604	4.9542
B6	SMR-DEP-500	943.6	4.6243	5.5047
B7	SMR-DEP-500	959.3	38.519	40.472
B8	SMR-DEP-500	942.0	3.7588	5.7351

**Table 5:** Allan deviation minima and values at  $\tau = 100ms$ . Devices marked with <sup>†</sup> are damaged.

For most devices, we observe the lowest noise somewhere between 0.1s and 1s, with the SMR-DEP-500 devices being an exception with minima between 0.01s and 0.1s. The entity of white and drift noises determines the exact position of the minimum[16].

The chips without electrodes seem to have less noise in average, but there is large variability between the devices (in particular, the A2, A3 and A7 chips are chipped outside of the bridge area, which might have affected the noise associated with them).

We also observe a disturbance at times shorter than 0.1s, present in only some of the measurements but maintaining the same shape in all of them, which could mean it is caused by noise from the read-out instrumentation. The effect is particularly visible in SMR-DEP-500 devices (see Fig. 16d).

**Resolution** The responsivity and the Allan noise can be used to obtain the mass resolution of the device if we know the frequency noise level: to resolve a mass change  $\Delta m$  with a duration  $\tau$  we need the corresponding frequency change  $\Delta\nu = \mathcal{R}\Delta m$  to be higher than the noise  $\nu_0\sigma_{Allan}(\tau)$  at the operation frequency  $\nu_0$ .

From the Allan deviation at  $\tau = 100ms$ , the corresponding air resonance frequencies in Table 5, and the lowest (in modulus) values of responsivity from the experimental results in Table 4 that have an associated air measurement, we can obtain a conservative estimate of the mass resolutions as  $-\nu_0\sigma_{Allan}/\mathcal{R}$ . The results are shown in Table 6.

## 6.4 Flow-through measurements with particles

Before testing the DEP trapping, some open loop measurements in flow-through mode (i.e. with particles passing through the resonator without being stopped) were performed, to test the ability of

Device	A4	A5	A6	A7	A8
Resolution(pg)	1.9661	1.7492	2.9864	1.6595	0.5761

**Table 6:** *Estimates for the mass resolutions at  $\tau = 100ms$ .*

the system to detect and measure the mass response due to particles, which for a particle that passes with constant velocity should be a peak with the same general shape as the resonator's first flexural mode function, but with width equal to the transit time.

Various pressure configurations were tested for the microfluidics system, with the objective of slowing the particles enough for the DEP trapping, while still having a sufficient number of them arrive to the junction.

Naming the inlet pressures  $\begin{pmatrix} P_1 & P_3 \\ P_2 & P_4 \end{pmatrix}$  based on their positions on the chip, the following configuration has been found to be effective: we keep  $P_4 = 0$ , then we increase  $P_1$  until we see enough particles passing and finally we raise  $P_2$  and  $P_3$ , using their ratio to control how many particles turn towards the bridge and the value of  $P_1 + P_2 - P_3$  to control their speed inside the resonator.

Our goal is to have transit times near the  $100ms$  "sweet spot", so it's easier to distinguish the actual response from the noise.

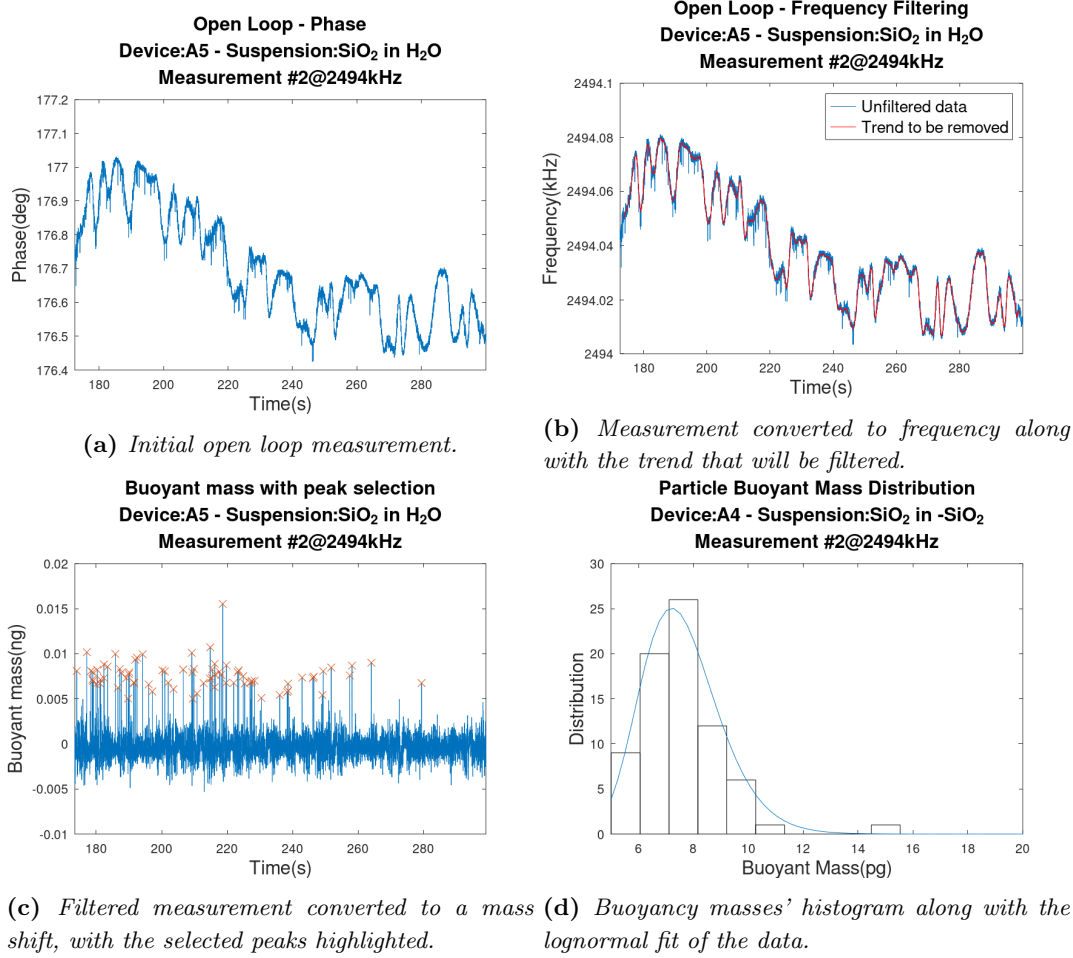
We performed measurements with water and ethanol solutions at different concentration (Pure  $H_2O$ , 25% $EtOH - H_2O$  and 50% $EtOH - H_2O$ ), with 3 different particle types:

- **ps8:** polystyrene analytical standard beads with an average diameter of  $\sim 8.13\mu m$ ;
- **SiO<sub>2</sub>:** silica analytical standard beads with an average diameter of  $\sim 5.29\mu m$ ;
- **mSiO<sub>2</sub>:** lab-made mesoporous silica beads with an average diameter of  $\sim 8\mu m$ ;

The measurement process is the following:

1. After filling the device with the same reference liquid used for the particle suspension we perform a sweep to find the resonance;
2. The fluid pressures are adjusted until particles start traversing the bridge at an acceptable speed; this is the most critical part of any measurement involving particles, because particles can get stuck along the walls of the channels (if the pressures are too low) or cluster together ultimately clogging the channels (if the pressures are too high);
3. One or multiple open loop measurements (Fig. 17a) are performed at the resonance frequency for the reference liquid, until enough data has been collected. During the measurement we record video of the bridge from the vibrometer camera to use as an additional reference during post-processing;
4. The open loop measurements are post-processed to extract the mass shifts caused by the particles: these should correspond to the difference between the particle's mass and that of the same volume of liquid. The post processing includes converting the data to frequency (in the same way as we did for the Allan deviation) and then to a mass shift (obtained using the theoretical responsivity  $\mathcal{R}_{theory} = -\nu_{air}/(2 * m_{air})$  corresponding to the nominal resonator mass of  $m_{air} = 1267ng$ ), applying a gaussian filter to remove the low frequency noise (Fig. 17b) and using Octave's `findpeaks` function to extract the peaks related to a particle's passage (Fig. 17c). Only peaks with heights and widths within specific ranges were selected to filter out peaks related to noise. Both these ranges and the filter parameters were chosen on a case-by-case basis in order to obtain the best selectivity.

5. The mass shifts' can now be analyzed statistically: we can group the peaks by measurement or particle/liquid combination, and apply a lognormal fit (which matches the expected mass distributions resulting from particle fabrication) to the resulting distributions (Fig. 17d). Histograms of the peaks grouped by particle suspension are plotted in Figure 18 along with the fitted distributions.
6. The statistical modes from the lognormal fits can be then plotted against the liquid densities (Fig. 19): a linear fit will then give us an estimate of the particle densities, masses and volumes, listed in Table 7.



**Figure 17:** Example processing steps for the flow through measurements.

**Results and observations** As said above, the post-processing parameters are a compromise between filtering the low frequency noise, preserving the peak heights and distinguishing the particle-related peaks from the high frequency noise, depending on the signal's characteristics; we can use the video recorded during the measurement to aid in identifying the correct peaks, but the mass resolution of the device remains an hard lower limit.

Figure 18 contains the histograms of the buoyant masses measured for each particle suspension along with a lognormal fit of the data. In most cases the distribution seem to be consistent with the expected lognormal behaviour, but it is difficult to distinguish a clear distribution for the measurements

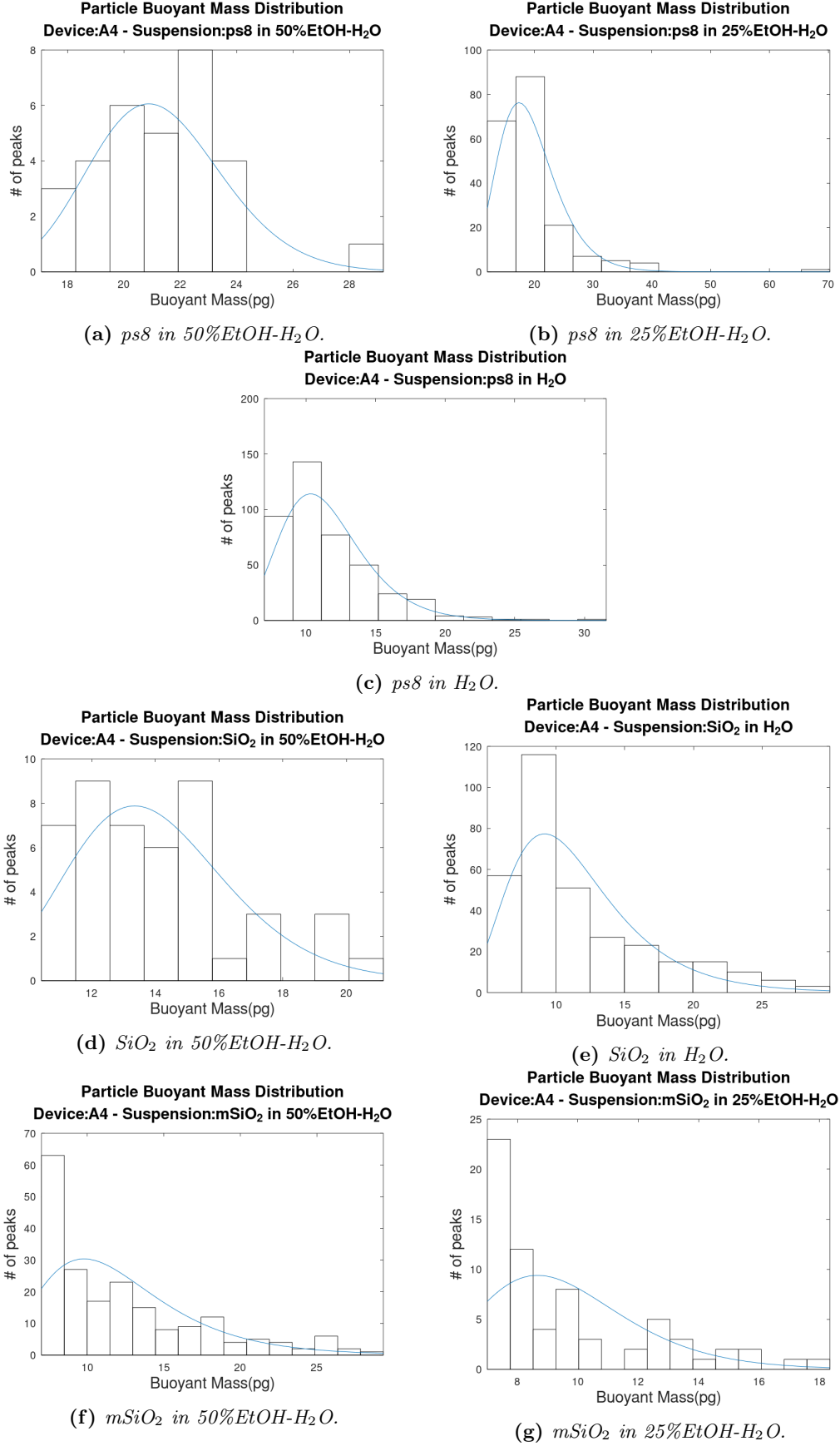
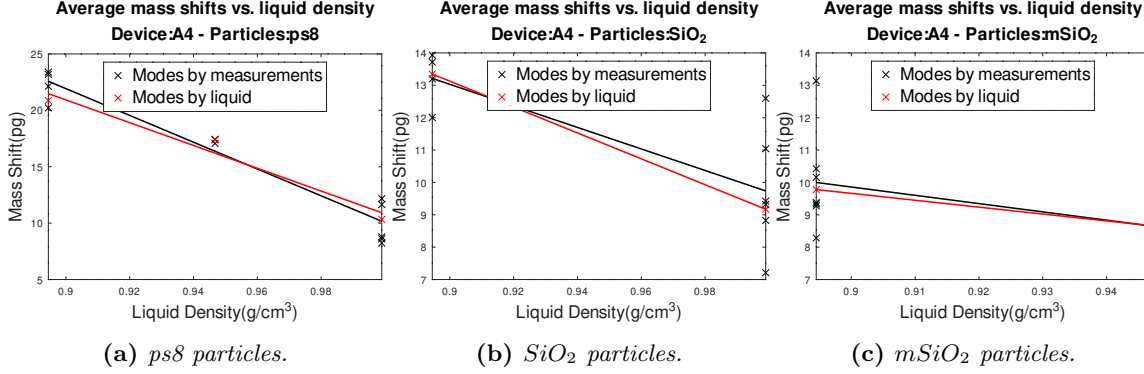


Figure 18: Buoyant masses histograms by solution.

with the mesoporous silica particles (Fig. 18f,18g), which feature a larger process variability than the standard particles, likely large enough to make the peak distribution overlap with the noise.



**Figure 19:** Modes for the fitted mass shifts plotted against liquid density and linearly fitted. The points "by measurement" are obtained by doing a lognormal fit for the peaks in each measurement, the values "by liquid" are obtained by doing the lognormal fits on all the peaks for each liquid.

The statistical modes from the lognormal fits are plotted against the liquid density in Fig. 19; a linear fit of these points gives us an estimate of the particle density and mass, listed in Table 7.

Particle	$\rho_{particle}(g/cm^3)$		$m_{particle}(pg)$	$V_{particle}(\mu m^3)$
	measured	nominal		
<i>ps8</i>	1.0846	1.05	111.83	101.01
<i>SiO<sub>2</sub></i>	1.2918	1.90	49.103	39.974
<i>mSiO<sub>2</sub></i>	1.2851	unknown	28.807	21.273

**Table 7:** Values of the particle mass, density and volume obtained from the statistical analysis of the peaks grouped by liquid. The "nominal" densities are from the particle datasheets.

From the results in Table 7 we can observe that similar densities are measured for the two types of silica based particles, but the estimated masses for the porous ones are correctly predicted to be much lower, meaning that the liquids are filling the particles' pores. These densities are significantly lower than the nominal value for the silica particles, likely because of smaller noise peaks getting mixed up in the measurement.

The polystyrene particles' densities have a better estimate, likely because of the better signal-to-noise ratio. This difference is also linked to the much wider mass distribution for the mesoporous silica particles, with the smaller particles below the noise limit.

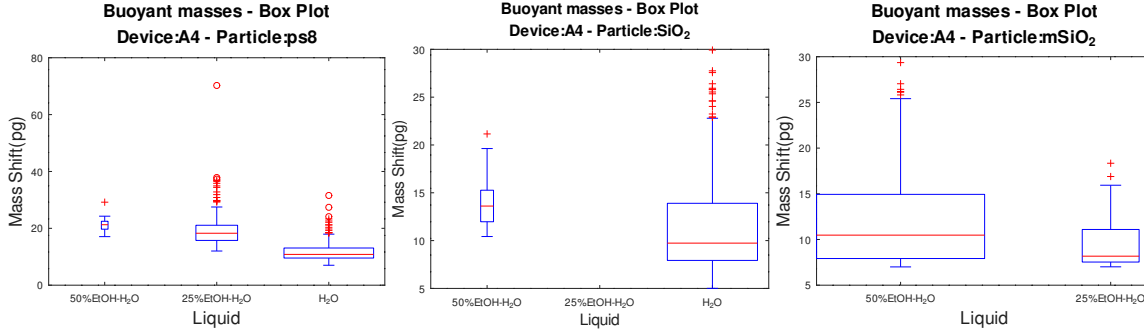
Even considering the effect of noise, we are still underestimating the real masses by a significant amount, which could have been caused by a failure to account for additional factors affecting the resonance and causing the actual responsivity to be lower than the theoretical value we used.

In fig. 20 we present the same data in box plot form, which provides more information relative to the same datasets:

- The boxes and the red lines inside them divide the dataset in 4 quarters with the same number of points: the red line is the median ( $Q_2$ ) and the box bounds are the first and third quartiles  $Q_1$  and  $Q_3$ .  $IQR = Q_3 - Q_1$  is known as the *interquartile range*;
- The boxes' widths are proportional to the number of points in their dataset;



- The "whiskers" further extend from the box bounds for a length of  $1.5 \cdot IQR$  (or to the furthest data point in that range): the points beyond them can be considered outliers;



**Figure 20:** Box plots of the mass shifts, grouped by liquid.

While we were able to find optimal parameters for the fluidic control and demonstrate the device's ability to detect the particle passage, further calibration of the device is needed if we want to use it to measure real masses.

## 6.5 DEP tests with particles

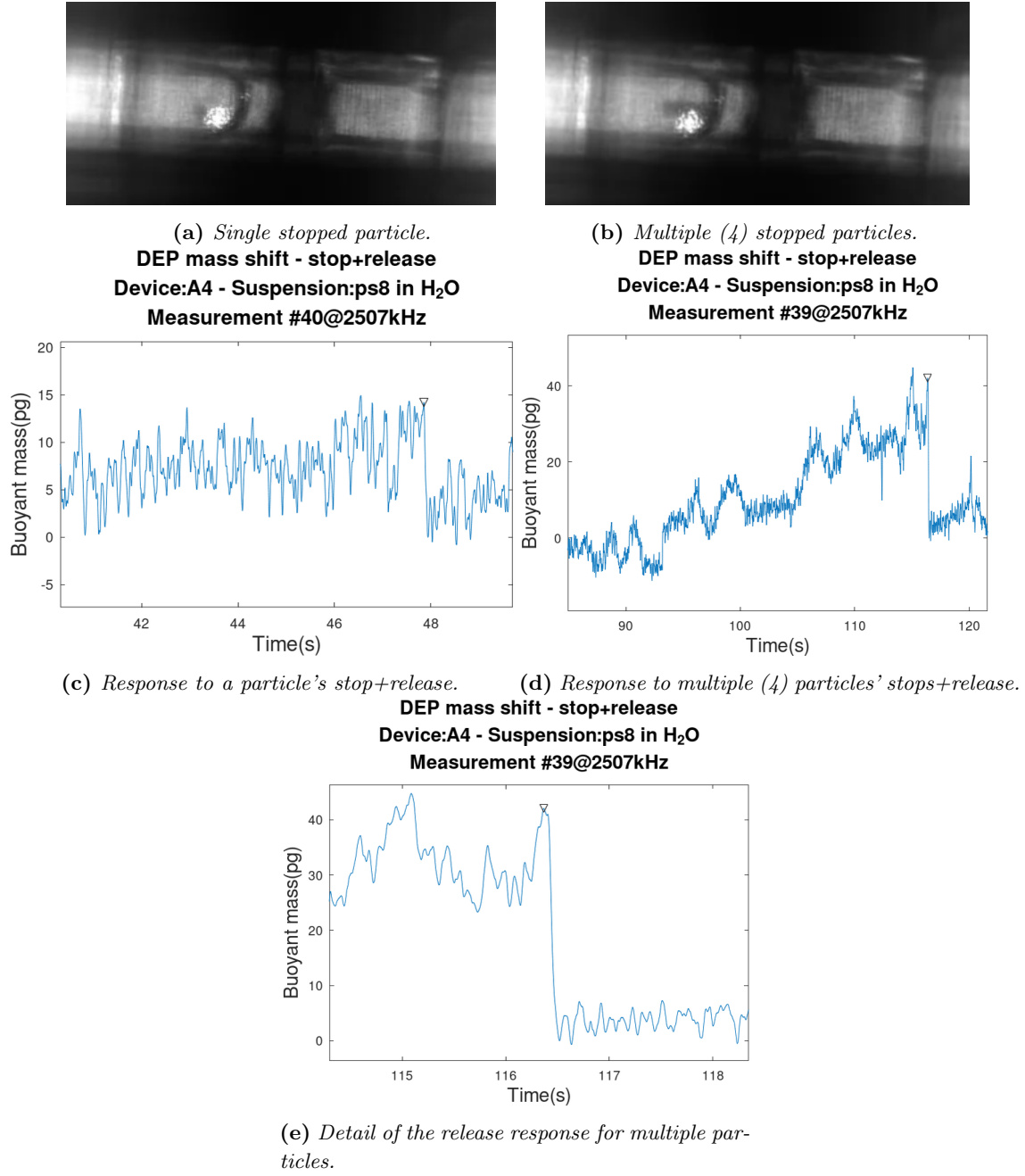
In this section we show the results of the tests of the DEP trapping, demonstrating the ability of the device to stop the particles and to exploit this trapping to obtain a more reliable measurement.

The measurement process is the same as the flowthrough case, with the following differences:

1. Once particles start passing through the resonator, we regulate the pressures to slow them as much as possible;
2. We start the open loop measurement and we apply a tension to the DEP electrodes, increasing it until we see particles stopping. As we can see in Figure 21a, the electrodes are designed to stop particles on one side, before they reach the bridge. If multiple particles are stopped consecutively, they accumulate in a "train", as shown in Figure 21b;
3. The data is converted to a mass shift as we did for the flow-through measurement;
4. We decrease the tension to release the particle(s): the measured mass shifts for the stop and release process is shown (for a single or multiple particles) in Figures 21c and 21d. While the gradual mass shift during the stop phase is lower and inconsistent (because of the uncentered and variable stopping point), as well as hard to measure because of the noise, when the particles are released we observe a peak (as the particles pass the point where the bridge response is highest, near the center) followed by a sharp decrease (Fig. 21e shows a detail of this response for multiple particles), whose height and width give us the buoyant mass (in the case of multiple particles we get the total for all particles) and the transit time through the second half of the resonator;
5. During the whole process we take note of parameters like the pressures and DEP tensions used and the stopping points.

**Results and observations** Table 8 summarizes all the information we have about the recorded events (we count each release of one or more particles as an event), including:

- The particle suspension;



**Figure 21:** *Particles stopped by DEP and corresponding measured mass shifts, the marked peaks correspond to the passage through the resonator's center.*

- The measured buoyant mass  $\Delta m$ ;
- The time to pass the second half of the bridge  $\Delta t_{L/2}$  and the corresponding average speed  $v_{L/2}$ ;
- The operating pressures  $P_n$ ;
- The DEP tension  $V_{stop}$  used to stop the particle and the  $V_{rel}$  at release. If the particle was released on its own (i.e. the trapping is unstable) both tensions are the same and we mark them accordingly;

- The number of particles  $N_p$ ;
- The stopping positions expressed as a fraction of the bridge length  $\bar{x}_{stop} = x_{stop}/L$ , a range refers to the positions of the first and last particle when there are multiple.

Suspension	$N_p$	$\Delta m (pg)$	$\Delta t_{L/2} (ms)$	$v_{L/2} (\mu m/s)$	$P_n (mbar)$	$V_{stop} (V)$	$V_{rel} (V)$	$\bar{x}_{stop}$
ps8 in $H_2O$	1	11.034	92.277	1354.62	$\begin{pmatrix} 25 & 40 \\ 15 & 0 \end{pmatrix}$	140*		0.14
	1	10.601	107.84	1159.11		180*		0.28
	1	13.106	134.52	929.200		140*		0.30
	1	13.221	66.706	1873.89		140*		0.28
	1	13.915	240.14	520.524		180*		0.24
	5	52.849	163.43	764.852		180	120	[0.15,0.28]
	3	36.370	137.86	906.719	$\begin{pmatrix} 30 & 40 \\ 15 & 0 \end{pmatrix}$	180	120	[0.22,0.30]
	1	12.141	102.28	1222.10		180	120	0.24
	1	12.224	100.06	1249.26		180	120	0.27
	1	11.498	78.936	1583.57		180*		0.24
	5	74.687	194.56	642.475		180*		[0.15,0.30]
	9	83.097	117.85	1060.69		180	168	[0.15,0.41]
	1	14.275	97.836	1277.65		180*		0.34
	1	9.6907	73.377	1703.53		180*		0.34
	1	13.465	144.53	864.871		180*		0.34
	1	13.157	113.40	1102.29		180*		0.35
	1	12.477	74.489	1678.11		180*		0.37
	1	12.093	142.31	878.384		180*		0.35
	1	15.340	124.52	1003.87		140*		0.26
	1	18.253	115.62	1081.09		140*		0.29
	13	100.18	118.96	1050.78		180	160	[0.06,0.52]
	4	42.073	152.31	820.680		180	160	[0.23,0.36]
	2	25.232	107.84	1159.11		180	160	[0.20,0.25]
	3	33.686	101.17	1235.53		180	160	[0.22,0.27]
	6	55.444	118.96	1050.78		180	160	[0.22,0.42]
	1	14.204	86.718	1441.45		180*		0.25
	1	16.158	135.64	921.583		180	160	0.40
	1	10.788	78.936	1583.57		180*		0.42
	1	14.168	162.32	770.090		180*		0.22
ps8 in 50%	1	27.904	464.72	268.979	$\begin{pmatrix} 80 & 120 \\ 70 & 0 \end{pmatrix}$	137.5*		0.24
EtOH- $H_2O$	3	40.820	152.31	820.680	$\begin{pmatrix} 100 & 140 \\ 80 & 0 \end{pmatrix}$	137.5*		[0.31,0.43]

**Table 8:** Summary of the data from the DEP trapping tests on the A4 device. The tensions marked with \* were not able to stop the particle(s) in a stable way, and the release happened before they were decreased.

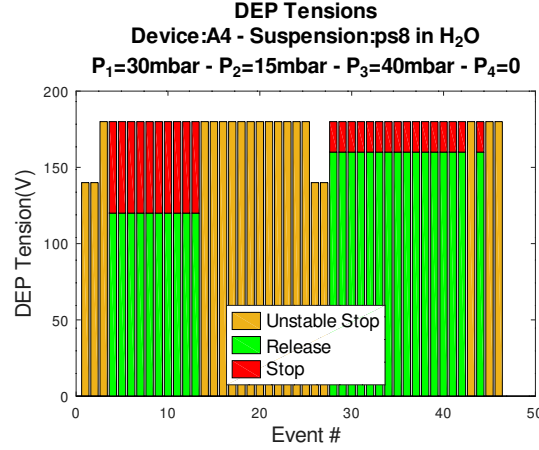
As Table 8 shows, we were only able to consistently achieve DEP trapping in the A4 device, with polystyrene particles and water. A very limited number of events was recorded in other conditions despite several attempts, and three main factors are to blame for this low reliability:

- The devices are susceptible to clogging when operated with particles, as the latter clump together in the channels blocking them, which in the worse cases can force a rebonding of the interface or even make the device permanently unusable;
- The speeds of the particles in the channel are very hard to control, with the same pressures producing very different result depending on the device, the suspension and the presence of damage or obstructions. That makes it very hard to apply the small pressure differences needed to slow down the particles enough for DEP trapping;
- The measurements had tight time constraints, mainly related to the use of the amplifier needed to apply a sufficient DEP tension.

The latter point is the main reason why ps8 particles in water were the most effective, as they proved easier to transport with lower, more stable pressures, making it easier to control both their rate

of arrival and their speed; the optimal equilibrium was found for  $P_1 = 30\text{mbar}$ ,  $P_2 = 15\text{mbar}$ ,  $P_3 = 40\text{mbar}$ , which allowed us to observe most of the trapping events.

In fact, we can observe that all the events where the particle was stopped in a stable manner (i.e. it was not released until the tension was reduced) used the same conditions: A4 device,  $P_1 = 30\text{mbar}$ ,  $P_2 = 15\text{mbar}$ ,  $P_3 = 40\text{mbar}$  pressures and ps8 particles in water. In Figure 22 we can see the tensions used to stop and release the particle in these conditions; we can observe that stable trapping always required a DEP tension of 180V, the highest we were able to apply with our setup.



**Figure 22:** Bar plot of the DEP stop and release tensions. The "Unstable Stop" bars refer to events where the particle released on its own.

This stable trapping was obtained only in about 52% of the events with an applied tension of 180V in the above conditions, suggesting that the DEP field is irregular and/or unstable, likely because of the fact that the electrodes and the underlying dielectric have a different shape (the irregular shape of the electrodes can be seen in Figure 21) because of overetching from the fabrication and gradual erosion during operation, both of which we talked about in previous sections.

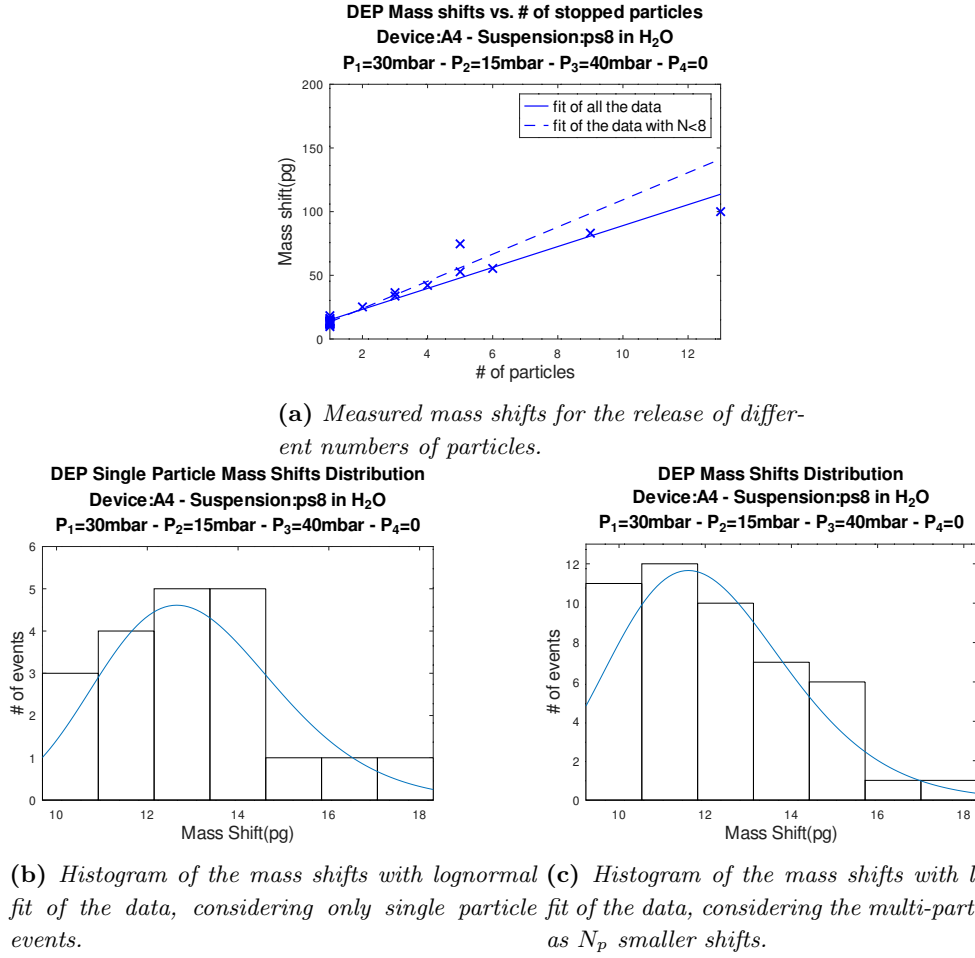
The stopping point should be near the center of the bridge, but the irregular field stops the particles before they reach the intended zone and often provides less stable trapping, explaining the low effectiveness of the trapping. Table 8 lists measurements (obtained from vibrometer camera images of the stopped particles) of the stopping positions as a fraction of the bridge length, which have values ranging between  $0.22L_{bridge}$  and  $0.42L_{bridge}$  for single particles.

Figure 23a shows the correlation between the jumps for the release of different numbers of particles, ideally we expect to measure the sum of the buoyant masses (we should therefore see a linear behaviour), but with many particles we observe a smaller value than expected as the particle "train" becomes longer and the particles keep each other from being fully weighted all at the same time.

As the fits in Figure 23a show, the effect is negligible for less than 8 particles, so the analysis on the mass shifts only has to ignore the events with 9 or more particles, and the remaining multi-particle mass shifts can be treated as many identical single-particle shifts.

Figures 23b shows the distribution of the buoyancy masses including only the single particle events, while Figure 23c also includes the multi-particle events, counting them as  $N_p$  identical shifts summing to the measured value. These distributions are relatively similar to the corresponding one in Figure 18c, but the latter has a second peak for lower mass shifts, which is likely caused by noise peaks we were not able to separate from the particle-related ones. The mode is also slightly smaller, which can also be attributed to noise, in this case low-frequency noise that forces us to apply an high pass filter to the data leading to an underestimation of the peak heights.

The ability to bypass both of these problems is a big advantage of the DEP approach: it is trivial



**Figure 23:** DEP mass shifts' analysis.

to find the correct jump as we know exactly when the particle is released, so high frequency noise has little or no effect, and the release is fast enough to negate the influence of low frequency noise (and remove the need for the high-pass filter).

## 7 Conclusions

In this work we demonstrated DEP trapping of microbeads in a glass SMR device, and its application for mass sensing purposes. The trapping uses coplanar electrodes fabricated with ion beam etching on top of the device, and the straight SMR bridge is made with a relatively simple femtosecond laser writing process, along with the microfluidic channels.

We characterized the resonance frequencies and Allan deviations when filled with air of four sets of devices, classified by the length of the bridge ( $250\mu m$  or  $500\mu m$ ) and by the presence or not of the DEP electrodes. The lowest Allan noise values were observed for averaging times between  $10ms$  and  $1s$ , and range in  $10^{-7} \div 10^{-6}$  for most devices. The devices with a  $250\mu m$  long bridge have lower masses with comparable minimum noise, so we expect them to have a better mass resolution, and only the devices with electrodes can perform DEP trapping: because of this, the measurements with liquids focused on the short bridge devices with DEP electrodes.

Resonance frequencies with different fluids inside the resonator were measured and linearly fitted against the fluid mass (predicted using the bridge nominal internal volume), which allowed us to estimate the responsivity and resonator mass when filled with air. Evaluating the resonance shifts has proven difficult as the peaks show irregular shapes and seem to be affected by multiple contributions, in some cases the measured shifts between liquid measurements were smaller than we would expect from the theory, corresponding to a lower (in modulus) effective responsivity.

The experimental responsivities range in the  $0.70 \div 1.21(kHz/ng)$  interval; for comparison, the theoretical responsivity values predicted from the air resonance frequencies by assuming a mass of  $1267ng$  (obtained from the nominal sizes and density of the resonator) range from  $1.05(kHz/ng)$  to  $1.08(kHz/ng)$ . This variability is partially caused by differences in the real mass of the resonators arising from a combination of process variability in the fabrication and gradual deterioration of the bridge electrodes.

Flow-through measurements were then attempted with standard polystyrene and silica beads and lab-made mesoporous silica particles, obtaining their buoyant masses in different liquids and fitting their statistical distributions with a lognormal distribution. A linear fit of the statistical modes against the density of the liquid allows us to estimate the density and mass of the particles, and therefore their volume. The measure predict densities of  $1.2918(g/cm^3)$ ,  $1.0846(g/cm^3)$  and  $1.2851(g/cm^3)$  respectively for silica, polystyrene and mesoporous silica particles, when the nominal values are  $1.90(g/cm^3)$  for the silica and  $1.05(g/cm^3)$  for the polystyrene. We obtain a better estimate of the density for the polystyrene particles, likely because of the better signal-to-noise ratio. Similar densities are predicted for the two types of silica based particles, but the estimated masses for the porous ones are correctly predicted to be much lower: this likely means that liquid is filling the particles' pores. The underestimation of the silica densities could be caused by noise peaks getting mixed up with particle peaks and lowering the average mass measurement.

Particle measurements were also used to find the most favorable particle suspension and microfluidic pressures for DEP trapping, slowing down the particles to stop without reducing their arrival rate at the resonator too much. Among the various liquid-particle dispersions, we were able to reliably achieve DEP trapping only for polystyrene particles in water. We obtained this result with a tension of  $180V$  for the DEP, with about 52% of the events stopping the particles in a stable manner. After releasing the particles by reducing the DEP tension, it is possible to measure the drop in the measured buoyant mass from the center point of the bridge (crossed after release) to the end. This approach circumvents high frequency noise as we know exactly when the particle is released, and the release is fast enough to make the influence of low frequency noise very small even without a filter.

The stopping point should be near the center of the bridge, but overetching under the electrodes causes bad adhesion near the edges, making those zones more susceptible to damage and in general altering their geometry: this results in an irregular electric field that can stops the particles before

they reach the intended zone and often provides less stable trapping.

While we were able to stop particles and use the trapping to obtain an improved buoyant mass measurement that is less influenced by the noise, the device still has significant problems: it is susceptible to clogging when operated with particles, the speed of the particles in the bridge is hard to control and the irregular trapping field causes reduced efficiency and an unreliable stopping position. Moreover, contributions other than the mass influence the resonance, significantly affecting the measurement. Many of these problems are caused or made worse by unwanted fabrication results such as overetching under the electrodes and channel wall roughness, therefore improving the fabrication process could significantly improve the device reliability and performance.

## Appendix: Post-processing with codes

Here we show the main Octave scripts that were used for post-processing along with a brief explanation of what they do. Auxiliary scripts that are not included here were used for data handling and plotting.

### Common scripts

These functions were used in multiple scripts to convert the phase open-loop measurement to frequency and/or apply a gaussian filter to detrend the data.

#### Phase fit

The `phase_fit` function performs a linear fit of the phase response from a sweep measurement, in a neighbourhood of a certain resonance frequency  $\nu_0$ . The obtained parameters can be used to convert the phase data from an open loop measurement performed at  $\nu_0$  to the corresponding frequency.

```

1 % function [fr_r,peak_max,fwhm,phase_slope,Q,ampl_fit] = f_lorentz(search_str,fwhm_0,
    fitsize)
2
3 function [Fit] = phase_fit(Sweep,X0,fitwidth)
4     kHz = 1e3;
5     mV = 1e-3;
6
7     if(exist ('OCTAVE_VERSION', 'builtin'))
8         pkg load optim;
9     end
10
11     X = Sweep.X;
12     ampl = Sweep.ampl;
13     phase = Sweep.phase;
14
15     fitrange = find((X>=(X0-0.5*fitwidth)) & (X<=(X0+0.5*fitwidth)));
16     adjusted_phase = unwrap(phase(fitrange)*(pi/180))*(180/pi);
17     phase_poly = polyfit(X(fitrange),adjusted_phase,1);
18
19     Q = abs(phase_poly(1))*X0/2;
20
21     Fit.X0 = X0;
22     Fit.Q = Q;
23     Fit.Xfit = X(fitrange);
24     Fit.phasefit = polyval(phase_poly,X(fitrange));
25     Fit.phasepoly = phase_poly;
26     Fit.phase0 = wrapTo180(polyval(phase_poly,X0));
27 end

```

#### Gaussian filter

The `gaussianfilter` function applies a gaussian filter to the input time-domain data, separating it in low and high frequency components for a time cutoff  $\tau$ . We used this to remove low frequency noise from the open-loop measurements.

```

1 function [waviness,roughness] = gaussianfilter(x,y,cutoff)
2
3 N = length(y);
4
5 dx = mean(diff(x));
6 n_cutoff = round(cutoff/dx);
7 t = (-n_cutoff-0.5:n_cutoff+0.5).*dx;
8

```



```

9 sigma = sqrt(log(2)/2)*cutoff/pi;
10 Hcdf = normcdf(t,0,sigma);
11 h = diff(Hcdf);
12
13 w = conv(y,flip1r(h),'valid');
14 y = y(1+n_cutoff:end-n_cutoff);
15 r = y - w;
16 %x = x(1+n_cutoff:end-n_cutoff)';
17
18 waviness = w;
19 roughness = r;
20
21 end

```

## Allan deviation

These scripts were used to obtain the Allan deviations from a series of open loop measurements.

### Main

The `main_allan` script converts the measurement to frequency and calls the `allanSTE` script to obtain the Allan deviation as a function of the averaging time. No high pass filter is used as we want to correctly estimate the low frequency noise.

```

1 clear all
2 close all
3
4 if(exist('OCTAVE_VERSION','builtin'))
5     pkg load statistics;
6 end
7
8 cm = 1e-2;
9 um = 1e-6;
10 kHz = 1e3;
11 mV = 1e-3;
12 ms = 1e-3;
13 ng = 1e-12;
14 g = 1e-3;
15
16 %% PARAMETERS %%
17 mainfolder = '../allan/chip_air_500';
18 plottersearch = 'meas_plotter*txt';
19 sweepsearch = 'meas_sweep*txt';
20 repeat_allan = false;
21
22 common_title = 'SMR-500 Devices - Air - Allan Deviation';
23 common_savename = 'SMR_500';
24 %%%%%%%%%%%%%%%
25
26 homefolder=pwd;
27 addpath(pwd); %In this way we can work on any folder
28
29 cd(mainfolder);
30 mainfolder=pwd;
31
32 sweeplist = ls2cell(sweepsearch);
33 plotterlist = ls2cell(plottersearch);
34
35 for i=1:length(sweeplist)
36     Buffer = read_simple(sweeplist{i});
37     Buffer.Fits = {};

```

```

38     Sweeps{i} = Buffer;
39 end
40
41 for i=1:length(plotterlist)
42     %parameters
43     fitsize = 10*kHz; %for phase fit
44
45     Buffer = read_simple(plotterlist{i});
46
47     i_sweep = sfind(Sweeps,'device',Buffer.device);
48     Buffer.i_sweep = i_sweep;
49     current_Sweep = Sweeps{i_sweep};
50
51     i_fit = sfind(current_Sweep.Fits,'X0',Buffer.X0);
52     if isempty(i_fit)
53         current_Sweep.Fits{end+1} = phase_fit(current_Sweep,Buffer.X0,fitsize); %phase_fit
54         i_fit = length(current_Sweep.Fits);
55     end
56     Buffer.i_fit = i_fit;
57     current_Fit = current_Sweep.Fits{i_fit};
58
59     Buffer.Yfreq = current_Fit.X0-(Buffer.Yphase-current_Fit.phase0)/current_Fit.
        phasepoly(1);
60
61     current_data.freq = Buffer.Yfreq;
62     current_data.int = mean(diff(Buffer.X));
63     current_data.rate = 1/current_data.int;
64     current_data.timeAcq = Buffer.X;
65
66     if repeat_allan
67         Buffer.Allan = allanSTE(current_data,30);
68         M=[Buffer.Allan.freq, Buffer.Allan.allan];
69         csvwrite(strcat('AllanSTE',Buffer.filename(13:end-20),'.csv'),M);
70     else
71         M=csvread(strcat('AllanSTE',Buffer.filename(13:end-20),'.csv'));
72         Buffer.Allan.freq = M(:,1);
73         Buffer.Allan.allan = M(:,2);
74     end
75
76     figure(1)
77     hold on
78     loglog(Buffer.Allan.freq, Buffer.Allan.allan,'DisplayName',Buffer.devname,'LineWidth
        ',1.5)
79
80     figure()
81     loglog(Buffer.Allan.freq, Buffer.Allan.allan)
82     title(strcat(Buffer.filename,'-Allan Deviation'),'Interpreter','none')
83     xlabel('Averaging time(s)')
84     ylabel('Allan Deviation')
85     current_savename = strrep(Buffer.filename,'.txt','-Allan.eps');
86     print(current_savename,'-depsc')
87     close
88
89     Plotters{i} = Buffer;
90 end
91
92 figure(1)
93 box on
94 title(common_title,'FontSize',15)
95 xlabel('Averaging time(s)','FontSize',15)
96 ylabel('Allan Deviation','FontSize',15)
97 xlim([current_data.int,10])

```

```

98 ylim([1e-7 5e-5])
99 current_savename = strcat(common_savename, '-Allan.eps');
100 legend('location','north','orientation','horizontal','FontSize',15)
101 print(current_savename, '-depsec')
102 %close
103
104 cd(homefolder)

```

## Calculation

The `allanSTE` function obtains the Allan deviation for each value of  $\tau = n\tau_0$  (where  $\tau_0$  is the sampling interval), by first averaging the data in groups of  $n$  consecutive samples and then obtaining the mean of the squared differences from the resulting averaged samples.

*(The credit for this script goes to Dr. Stassi)*

```

1 %optimized
2 function [ avarSTE ] = allanSTE(data,varargin)
3 disp('AllanSte')
4 tic;
5 fr=data.freq;
6 f0=mean(fr);
7 %tempo step
8 tau=data.int;
9 %tau=mean(int);
10 %sec=time(end)
11 %numero di acquisizioni
12 step=length(fr);
13 sec=tau*step;
14
15 if nargin >= 2
16     sec = 2*varargin{1};
17     step = min(floor(sec/tau),step);
18 end
19 %n=1;
20 %i=1;
21 %allan_dev=0;
22 flag=0;
23 for n=1:step
24     check2=floor(step/n);
25     if check2>1
26         flag=flag+1;
27     end
28 end
29
30 x=zeros(flag,1);
31 totale=zeros(flag,1);
32 allan_dev=zeros(flag,1);
33
34 for n=1:flag
35     check=floor(step/n);
36     fr_new=zeros(check,1);
37     c=1;
38
39     %calcolo dei nuovi vettori
40     for i=1:check
41         a=c+n-1;
42         fr_new(i)=mean(fr(c:a));
43         c=c+n;
44     end
45     x(n)=n*tau;
46     %fx(n)=fr_new;

```

```

47     tot=0;
48
49     %somma delle differenze quadratiche fra ogni step
50     for j=2:check
51         tot = tot + ((fr_new(j)-fr_new(j-1))/f0)^2;
52     end
53     %calcolo allan deviation
54     totale(n)=tot;
55     allan_dev(n)=sqrt((1/(2*(check)-2))* tot);
56 end
57
58 avarSTE.allan=allan_dev;
59 avarSTE.freq=x;
60 toc;
61 end

```

## Flow-through measurements

The following scripts were used to find and analyze the mass peaks from flow-through particle measurements.

### Main

The `main_particles` scripts (with slightly different variants for each particle type) convert the open loop measurements to frequency, apply a gaussian filter and use the theoretical responsivities to convert the results to mass shifts. The `find_particles` function is called to handle the peak detection. The peaks are classified and the distributions for each condition are obtained, then a lognormal fit of the data is performed. The modes are then linearly fitted against the liquid densities to estimate densities and real masses of the particles.

```

1  clear all
2  close all
3
4  if(exist ('OCTAVE_VERSION', 'builtin'))
5      pkg load statistics;
6  end
7
8  cm = 1e-2;
9  um = 1e-6;
10 kHz = 1e3;
11 mV = 1e-3;
12 ms = 1e-3;
13 ng = 1e-12;
14 pg = 1e-15;
15 g = 1e-3;
16
17 %% PARAMETERS %%
18 mainfolder = '../ps8';
19 %searchstr = {'meas_open*_*_.txt'}; %Starting with meas_open is advised, as the
    %script will find the latest sweep files on its own
20 %excludebad = false;
21 %exclude_conditions = {'disturbed'};
22 %exclude_highTC = false;
23 mair = 1267*ng; %empty mass
24 mh2o = 205*ng;
25 dh2o = 0.999*g/cm^3;
26 metOH = 162*ng;
27 detOH = 0.790*g/cm^3;
28
29 psize = 8.13*um;

```

```

30
31 Nbars = 10;
32
33 plottersearch = 'meas_plotter*txt';
34 sweepsearch = 'meas_sweep*txt';
35 %%%%%%%%%%%%%
36
37 homefolder=pwd;
38 addpath(pwd); %In this way we can work on any folder
39
40 cd(mainfolder);
41 mainfolder=pwd;
42 subfoldersearch = '*';
43 folderlist = dir2cell(subfoldersearch);
44
45 Avg_by_meas = [];
46
47 Avg_by_liq(1,:) = dh2o*[0:0.25:1]+detOH*flipplr([0:0.25:1]);
48 %Sum_by_liq = zeros(1,5);
49 %Npart_liq = zeros(1,5);
50
51 Particles_all = [];
52 Particles_by_liq = {[],[],[],[],[]];
53
54 for i_folder = 1:length(folderlist)
55     cd(folderlist{i_folder});
56     sweeplist = ls2cell(sweepsearch);
57     plotterlist = ls2cell(plottersearch);
58
59     for i=1:length(sweeplist)
60         Buffer = read_simple(sweeplist{i});
61
62         figure()
63         box on
64         subplot(2,1,1)
65         plot(Buffer.X/kHz,Buffer.ampl/mV)
66         title(Buffer.filename, 'Interpreter', 'none')
67         xlabel('Frequency(kHz)')
68         ylabel('Amplitude(mV)')
69         subplot(2,1,2)
70         plot(Buffer.X/kHz,Buffer.phase)
71         xlabel('Frequency(kHz)')
72         ylabel('Phase(deg)')
73         ylim([-180,180])
74         print(strrep(Buffer.filename,'txt','eps'),'-depsc')
75         close
76
77         Buffer.Fits = {};
78
79         Sweeps{i} = Buffer;
80     end
81
82     for i=1:length(plotterlist)
83         %parameters
84         fitsize = 10*kHz; %for phase fit
85         cutoff = 2; %for filter
86
87         %particle constraints
88         minw = 25*ms; %duration of passage
89         maxw = cutoff;
90         mind = 0;
91         minh_m = 0.007*ng;

```

```

92     maxh_m = 0.03*ng;
93
94
95     Buffer = read_simple(plotterlist{i});
96
97     current_title = strrep(strcat(Buffer.device(1:end-2),'-',Buffer.condition),'-CUT',
98     '');
99     post_title = strcat('#',Buffer.ID);
100
101     TS = Buffer.X(2)-Buffer.X(1);
102
103     figure()
104     plot(Buffer.X,Buffer.Yphase)
105     title(strcat(current_title,'-Open Loop @',num2str(Buffer.X0/kHz),'kHz-',post_title
106     ))
107     xlabel('Time(s)')
108     ylabel('Phase(deg)')
109     xlim(Buffer.X([1,end]))
110     current_savename = strrep(Buffer.filename,'txt','eps');
111     print(current_savename,'-depsec')
112     close
113
114     i_sweep = intersect(sfind(Sweeps,'device',Buffer.device),sfind(Sweeps,'condition',
115     strrep(Buffer.condition,'-CUT','')));
116     timestamps = cellfun('getfield',Sweeps(i_sweep),repmat({'timestamp'},1,length(
117     i_sweep)));
118     [~,i_sweep] = min(abs(timestamps-Buffer.timestamp)); %index of sweep
119     Buffer.i_sweep = i_sweep;
120
121     current_Sweep = Sweeps{i_sweep};
122
123     i_fit = sfind(current_Sweep.Fits,'X0',Buffer.X0);
124     if isempty(i_fit)
125         current_Sweep.Fits{end+1} = phase_fit(current_Sweep,Buffer.X0,fitsize); %
126         phase_fit
127         i_fit = length(current_Sweep.Fits);
128     end
129     Buffer.i_fit = i_fit;
130
131     current_Fit = current_Sweep.Fits{i_fit};
132
133     Buffer.Yfreq = current_Fit.X0-(Buffer.Yphase-current_Fit.phase0)/current_Fit.
134     phasepoly(1);
135     [~,Buffer.Yfreq_filtered] = gaussianfilter(Buffer.X,Buffer.Yfreq,cutoff);
136     Buffer.Yfreq_filtered = Buffer.Yfreq_filtered;
137     cut_size = (length(Buffer.Yfreq)-length(Buffer.Yfreq_filtered))/2;
138     Buffer.Xcut = Buffer.X(cut_size+1:end-cut_size);
139     Yfreq_cut = Buffer.Yfreq(cut_size+1:end-cut_size);
140
141     figure()
142     plot(Buffer.X,Buffer.Yfreq/kHz)
143     title(strcat(current_title,'-O.L. @',num2str(Buffer.X0/kHz),'kHz-',post_title,'-
144     Frequency'))
145     xlabel('Time(s)')
146     ylabel('Frequency(kHz)')
147     xlim(Buffer.X([1,end]))
148     print(strrep(current_savename,'.','_Freq'),'_depsec')
149     close
150
151     figure()
152     plot(Buffer.Xcut,Buffer.Yfreq_filtered/kHz)

```

```

146     title(strcat(current_title, '-0.L. @', num2str(Buffer.X0/kHz), 'kHz-', post_title, '-
Frequency Shift-Filtered'))
147     xlabel('Time(s)')
148     ylabel('Frequency Shift(kHz)')
149     xlim(Buffer.Xcut([1, end]))
150     print(strrep(current_savename, '.', '_Freq-filt.'), '-depsc')
151     close
152
153     figure()
154     plot(Buffer.X, Buffer.Yfreq/kHz)
155     hold on
156     plot(Buffer.Xcut, (Yfreq_cut-Buffer.Yfreq_filtered)/kHz, 'r')
157     %plot(Buffer.Xcut, Buffer.Yfreq_filtered/kHz)
158     title(strcat(current_title, '-0.L. @', num2str(Buffer.X0/kHz), 'kHz-', post_title, '-
Frequency Shift-Difference'))
159     xlabel('Time(s)')
160     ylabel('Frequency Shift(kHz)')
161     xlim(Buffer.X([1, end]))
162     print(strrep(current_savename, '.', '_Freq-filt-diff.'), '-depsc')
163     close
164
165     current_conds = strsplit(Buffer.condition, {'+', '-'});
166     switch current_conds{1}
167         case 'h2o'
168             n_liq = 5;
169             Buffer.m0 = mair+mh2o;
170             Buffer.dliquid = dh2o;
171             if Buffer.ID == '4' || Buffer.ID == '7'
172                 minh_m = 0.01*ng;
173             end
174             if Buffer.ID == '4'
175                 maxh_m = 0.06*ng;
176             end
177             if Buffer.ID == '36'
178                 maxh_m = 0.015*ng;
179             end
180         case 'etOH'
181             n_liq = 1;
182             Buffer.m0 = mair+metOH;
183             Buffer.dliquid = detOH;
184             minh_m = 0.01*ng;
185             maxh_m = 0.06*ng;
186         case '25etOH'
187             n_liq = 4;
188             Buffer.m0 = mair+0.25*metOH+0.75*mh2o;
189             Buffer.dliquid = 0.25*detOH+0.75*dh2o;
190             minh_m = 0.012*ng;
191             maxh_m = 0.1*ng;
192         case '50etOH'
193             n_liq = 3;
194             Buffer.m0 = mair+0.5*metOH+0.5*mh2o;
195             Buffer.dliquid = 0.5*detOH+0.5*dh2o;
196             minh_m = 0.015*ng;
197             if Buffer.ID == '47'
198                 maxh_m = 0.06*ng;
199             end
200         case '75etOH'
201             n_liq = 2;
202             Buffer.m0 = mair+0.75*metOH+0.25*mh2o;
203             Buffer.dliquid = 0.75*detOH+0.25*dh2o;
204     end
205

```

```

206 Buffer.Ypmass = -2*Buffer.m0*(Buffer.Yfreq-current_Fit.X0)./(current_Fit.X0); %
    this is only actually valid for the peaks!!
207 Buffer.Ypmass_filtered = -2*Buffer.m0*(Buffer.Yfreq_filtered)./(current_Fit.X0);
208
209 figure()
210 plot(Buffer.X,Buffer.Ypmass/pg)
211 title(strcat(current_title,'-0.L. @',num2str(Buffer.X0/kHz),'kHz-',post_title,'-
    Mass Shift'))
212 xlabel('Time(s)')
213 ylabel('Mass Shift(pg)')
214 xlim(Buffer.X([1,end]))
215 print(strrep(current_savename, '.', '_pmass.'), '-depsc')
216 close
217
218 figure()
219 plot(Buffer.Xcut,Buffer.Ypmass_filtered/pg)
220 title(strcat(current_title,'-0.L. @',num2str(Buffer.X0/kHz),'kHz-',post_title,'-
    Mass Shift-Filtered'))
221 xlabel('Time(s)')
222 ylabel('Mass Shift(pg)')
223 xlim(Buffer.Xcut([1,end]))
224 print(strrep(current_savename, '.', '_pmass-filt.'), '-depsc')
225 close
226
227 % if ~isempty(strfind(Buffer.condition,'ps8'))
228 %     Buffer.dparticle = 1.05*g/cm^3;
229 % elseif ~isempty(strfind(Buffer.condition,'msio'))
230 %     Buffer.dparticle = 2*g/cm^3;
231 % elseif ~isempty(strfind(Buffer.condition,'siox'))
232 %     Buffer.dparticle = 1.9*g/cm^3;
233 % end
234
235 %dfloating = [min_dp,max_dp]-Buffer.dliquid;
236 %minh_m = dfloating(1)*(4/3)*pi*(psize/2)^3;
237 %maxh_m = dfloating(2)*(4/3)*pi*(psize/2)^3;
238
239 Buffer.Particles = find_particles(Buffer.Xcut,Buffer.Ypmass_filtered,[minh_m,
    maxh_m],[floor(minw/TS),ceil(maxw/TS)],floor(mind/TS));
240
241 %remove hits from cuts
242 if ~isempty(strfind(Buffer.filename,'CUT'))
243     j=1;
244     while j<=length(Buffer.Particles.loc)
245         current_loc = Buffer.Particles.loc(j);
246         pre = Buffer.Xcut(current_loc) - Buffer.Xcut(current_loc-1);
247         post = Buffer.Xcut(current_loc+1) - Buffer.Xcut(current_loc);
248         if abs(pre-TS)>=1e-6 || abs(post-TS)>=1e-6
249             Buffer.Particles.loc(j) = [];
250             Buffer.Particles.pks(j) = [];
251         end
252         j=j+1;
253     end
254 end
255
256 figure()
257 plot(Buffer.Xcut,Buffer.Ypmass_filtered/pg)
258 hold on
259 plot(Buffer.Xcut(Buffer.Particles.loc),Buffer.Particles.pks/pg,'x')
260 title(strcat(current_title,'-0.L. @',num2str(Buffer.X0/kHz),'kHz-',post_title,'-
    Mass Shift-Particles'))
261 xlabel('Time(s)')
262 ylabel('Mass Shift(pg)')

```



```

263 xlim(Buffer.Xcut([1,end]))
264 print(strrep(current_savename, '.', '_pmass-filt+fit.'), '-depsc')
265 %close
266
267 Buffer.Particles.freqs = -0.5*(Buffer.Particles.pks/Buffer.m0).*(current_Fit.X0);
268 Buffer.Particles.denp = (6*Buffer.Particles.pks)/(pi*psize^3)+Buffer.dliquid;
269 %Buffer.Particles.masses = Buffer.Particles.pks.*(Buffer.Particles.denp)./(Buffer.
    Particles.denp-Buffer.dliquid);
270 N_particles = length(Buffer.Particles.pks);
271
272 if ~isempty(Buffer.Particles.freqs)
273 %
274 % figure()
275 % hist(Buffer.Particles.masses/pg,1000);
276 % title(strcat(Buffer.filename, '-Mass Distribution'), 'Interpreter', 'none')
277 % xlabel('Particle Mass(pg)')
278 % ylabel('Distribution')
279 % print(strrep(current_savename, '.', '_mdistr.'), '-depsc')
280 % close
281 %
282 % figure()
283 % hist(Buffer.Particles.sizes/um,1000);
284 % title(strcat(Buffer.filename, '-Size Distribution'), 'Interpreter', 'none')
285 % xlabel('Particle Size(um)')
286 % ylabel('Distribution')
287 % %print(strrep(current_savename, '.', '_sizedistr.'), '-depsc')
288 % close
289 %
290 % figure()
291 % hist(Buffer.Particles.freqs/kHz,1000);
292 % title(strcat(Buffer.filename, '-Freq. Shift Distribution'), 'Interpreter', 'none
    ')
293 % xlabel('Frequency Shift(um)')
294 % ylabel('Distribution')
295 % %print(strrep(current_savename, '.', '_freqdistr.'), '-depsc')
296 % close
297
298 [pks_m_logn,pks_s_logn] = logn_fit(Buffer.Particles.pks);
299 pks_mode = exp(pks_m_logn-pks_s_logn^2);
300 current_avg = [Buffer.dliquid;pks_mode];
301 Avg_by_meas = [Avg_by_meas,current_avg];
302
303 Particles_all = [Particles_all,Buffer.Particles.pks];
304 Particles_by_liq{n_liq} = [Particles_by_liq{n_liq},Buffer.Particles.pks];
305
306 %Sum_by_liq(n_liq) = Sum_by_liq(n_liq) + sum(Buffer.Particles.pks);
307 %lnSum_by_liq(n_liq) = lnSum_by_liq(n_liq) + sum(log(Buffer.Particles.pks));
308 %Npart_liq(n_liq) = Npart_liq(n_liq) + N_particles;
309
310 figure()
311 hold on
312 hist(Buffer.Particles.pks/pg,Nbars,'facecolor','w');
313 xtemp = linspace(minh_m,maxh_m,100);
314 %ytemp = (mean(histc(Buffer.Particles.pks,linspace(min(Buffer.Particles.pks),max
    (Buffer.Particles.pks),Nbars+1)))/mean(lognpdf(xtemp,pks_m_logn,pks_s_logn)))*
    lognpdf(xtemp,pks_m_logn,pks_s_logn);
315 ytemp = (N_particles/Nbars)*(maxh_m-minh_m)*lognpdf(xtemp,pks_m_logn,pks_s_logn)
    ;
316 plot(xtemp/pg,ytemp)
317 title(strcat(current_title, '-0.L. @', num2str(Buffer.X0/kHz), 'kHz-', post_title, '-
    Particle Mass Shifts-Distribution'))
318 xlabel('Buoyant Mass(pg)')
319 ylabel('Distribution')

```

```

319     print(strrep(current_savename, '.', '_pkdistr.'), '-depsc')
320     %close
321
322     freq_m_logn = pks_m_logn+log(current_Fit.X0/(2*Buffer.m0));
323     freq_s_logn = pks_s_logn;
324     minfreq = -maxh_m*(current_Fit.X0/(2*Buffer.m0));
325     maxfreq = -minh_m*(current_Fit.X0/(2*Buffer.m0));
326
327     % figure()
328     % hold on
329     hist(Buffer.Particles.freqs/kHz,Nbars,'facecolor','w');
330     % xtemp = linspace(minfreq,maxfreq,100);
331     % ytemp = (N_particles/Nbars)*(maxfreq-minfreq)*lognpdf(-xtemp,freq_m_logn,
freq_s_logn);
332     % plot(xtemp/kHz,ytemp)
333     % title(strcat(current_title,'-0.L. @',num2str(Buffer.X0/kHz),'kHz-',post_title
,'-Particle Frequency Shifts-Distribution'))
334     % xlabel('Frequency Shift(um)')
335     % ylabel('Distribution')
336     % print(strrep(current_savename, '.', '_freqdistr.'), '-depsc')
337     % close
338
339     denf_m_logn = pks_m_logn+log(6/(pi*psize^3));
340     denf_s_logn = pks_s_logn;
341     min_dp = (6*minh_m)/(pi*psize^3)+Buffer.dliquid;
342     max_dp = (6*maxh_m)/(pi*psize^3)+Buffer.dliquid;
343
344     % figure()
345     % hold on
346     % hist(Buffer.Particles.denp/(g/cm^3),Nbars,'facecolor','w');
347     % xtemp = linspace(min_dp,max_dp,100);
348     % ytemp = (N_particles/Nbars)*(max_dp-min_dp)*lognpdf(xtemp-Buffer.dliquid,
denf_m_logn,denf_s_logn);
349     % plot(xtemp/(g/cm^3),ytemp)
350     % title(strcat(current_title,'-0.L. @',num2str(Buffer.X0/kHz),'kHz-',post_title
,'-Particle Densities-Distribution'))
351     % xlabel('Particle Density(pg)')
352     % ylabel('Distribution')
353     % print(strrep(current_savename, '.', '_denpdistr.'), '-depsc')
354     % close
355
356     % mass_m_logn = pks_m_logn+log(Buffer.dparticle/dfloating);
357     % mass_s_logn = pks_s_logn;
358     % figure()
359     % hold on
360     % hist(Buffer.Particles.sizes/um,Nbars,Nbars/(maxsize-minsize));
361     % xtemp = linspace(minsize,maxsize,1000);
362     % plot(xtemp/um,lognpdf(xtemp,size_m_logn,size_s_logn))
363     % title(strcat(Buffer.filename,'-Size Distribution-Fitted'), 'Interpreter', 'none
'),
364     % xlabel('Particle Size(um)')
365     % ylabel('Distribution')
366     % print(strrep(current_savename, '.', '_mdistr.'), '-depsc')
367     % close
368
369
370
371     else
372         warning('no particles detected')
373     end
374     %Plotters{i} = Buffer;
375 end

```

```

376     cd(mainfolder);
377 end
378
379 %Sum_by_liq(find(Npart_liq==0))=[];
380 %Avg_by_liq(:,find(Npart_liq==0))=[];
381 %Npart_liq(find(Npart_liq==0))=[];
382
383 %Avg_by_liq(2,:) = Sum_by_liq./Npart_liq;
384
385 cd(homefolder)
386
387 %figure()
388 %plot(Avg_by_meas(1,:)/(g/cm^3),Avg_by_meas(2,:)/pg,'x');
389 %title('ps8 - Average mass shifts')
390 %xlabel('Liquid Density(g/cm^3)')
391 %ylabel('Mass Shift(pg)')
392 %xlim([min(Avg_by_meas(1,:)),max(Avg_by_meas(1,:))]/(g/cm^3))
393 %print('ps8_avgfit.eps','-depsc')
394 %%close
395
396 avgfit = polyfit(Avg_by_meas(1,:),Avg_by_meas(2,:),1);
397
398 figure()
399 plot(Avg_by_meas(1,:)/(g/cm^3),Avg_by_meas(2,:)/pg,'kx');
400 hold on
401 plot(linspace(min(Avg_by_meas(1,:)),max(Avg_by_meas(1,:)),100)/(g/cm^3),polyval(avgfit
    ,linspace(min(Avg_by_meas(1,:)),max(Avg_by_meas(1,:)),100))/pg,'k');
402 title('ps8 - Average mass shifts - Fitted')
403 xlabel('Liquid Density(g/cm^3)')
404 ylabel('Mass Shift(pg)')
405 xlim([min(Avg_by_meas(1,:)),max(Avg_by_meas(1,:))]/(g/cm^3))
406 print('ps8_avgfit-fitted.eps','-depsc')
407 %close
408
409 [pks_m_all,pks_s_all] = logn_fit(Particles_all);
410 pks_mode_all = exp(pks_m_all-pks_s_all^2);
411 dlmwrite('p_ps8_all.txt',Particles_all')
412
413 liq_savenames = {'p_ps8_etOH.txt','p_ps8_75etOH_h2o.txt','p_ps8_50etOH_h2o.txt','
    p_ps8_25etOH_h2o.txt','p_ps8_h2o.txt'};
414 for i = 1:length(Particles_by_liq)
415     if ~isempty(Particles_by_liq{i})
416         [pks_m_liq(i),pks_s_liq(i)] = logn_fit(Particles_by_liq{i});
417         pks_mode_liq(i) = exp(pks_m_liq(i)-pks_s_liq(i)^2);
418         dlmwrite(liq_savenames{i},Particles_by_liq{i}')
419     else
420         pks_mode_liq(i) = 0;
421     end
422 end
423
424 Avg_by_liq(2,:) = pks_mode_liq;
425 Avg_by_liq(:,find(pks_mode_liq==0))=[];
426
427 avgfit_liq = polyfit(Avg_by_liq(1,:),Avg_by_liq(2,:),1);
428
429 figure()
430 plot(Avg_by_meas(1,:)/(g/cm^3),Avg_by_meas(2,:)/pg,'kx','DisplayName','Modes by
    measurements');
431 hold on
432 plot(linspace(min(Avg_by_meas(1,:)),max(Avg_by_meas(1,:)),100)/(g/cm^3),polyval(avgfit
    ,linspace(min(Avg_by_meas(1,:)),max(Avg_by_meas(1,:)),100))/pg,'k',
    'HandleVisibility','off','LineWidth',1.5);

```

```

433 plot(Avg_by_liq(1,:)/(g/cm^3),Avg_by_liq(2,:)/pg,'rx','DisplayName','Modes by liquid')
434 ;
435 plot(linspace(min(Avg_by_liq(1,:)),max(Avg_by_liq(1,:)),100)/(g/cm^3),polyval(
    avgfit_liq,linspace(min(Avg_by_liq(1,:)),max(Avg_by_liq(1,:)),100))/pg,'r',
    'HandleVisibility','off','LineWidth',1.5);
436 title({'Average mass shifts vs. liquid density','Device:A4 - Particles:ps8'},'FontSize',15)
437 xlabel('Liquid Density(g/cm^3)','FontSize',15)
438 ylabel('Mass Shift(pg)','FontSize',15)
439 xlim([min(Avg_by_liq(1,:)),max(Avg_by_liq(1,:))]/(g/cm^3))
440 legend('Location','north','FontSize',13)
441 print('ps8_avgfit-liq-fitted.eps','-depsc')
442 %close
443
444 labels = {'EtOH','75%EtOH-H_2O','50%EtOH-H_2O','25%EtOH-H_2O','H_2O'};
445 labels_sv = {'etOH','75etOH-h2o','50etOH-h2o','25etOH-h2o','h2o'};
446
447 figure()
448 boxplot(cellfun(@(x) x./pg,Particles_by_liq,'UniformOutput',false))
449 xticks([1,2,3,4,5])
450 xticklabels(labels)
451 title({'Buoyant masses - Box Plot','Device:A4 - Particle:ps8'},'FontSize',15)
452 xlabel('Liquid','FontSize',15)
453 ylabel('Mass Shift(pg)','FontSize',15)
454 print('ps8_liq-boxplot.eps','-depsc')
455 %close
456
457 for i_l = 1:length(Particles_by_liq)
458     Mbars = 10;
459     if ~isempty(Particles_by_liq{i_l})
460         figure()
461         hold on
462         box on
463         hist(Particles_by_liq{i_l}/pg,Mbars,'facecolor','w');
464         xtemp = linspace(min(Particles_by_liq{i_l}),max(Particles_by_liq{i_l}),100);
465         [pks_m_logn,pks_s_logn] = logn_fit(Particles_by_liq{i_l});
466         ytemp = (mean(histc(Particles_by_liq{i_l},linspace(min(Particles_by_liq{i_l}),
            max(Particles_by_liq{i_l}),Mbars+1))/mean(lognpdf(xtemp,pks_m_logn,pks_s_logn)))*
            lognpdf(xtemp,pks_m_logn,pks_s_logn));
467         %ytemp = (length(Particles_by_liq{i_l})/Mbars)*(maxh_m-minh_m)*lognpdf(xtemp,
            pks_m_logn,pks_s_logn);
468         plot(xtemp/pg,ytemp)
469         title({'Particle Buoyant Mass Distribution',[Device:A4 - Suspension:ps8 in ',
            labels{i_l}]],'FontSize',15)
470         xlabel('Buoyant Mass(pg)','FontSize',15)
471         ylabel('# of peaks','FontSize',15)
472         xlim([min(Particles_by_liq{i_l}),max(Particles_by_liq{i_l})]/pg)
473         print(strcat('ps8_',labels_sv{i_l},'_pkdistr.eps'),'depsc')
474         %close
475     end
476 end
477
478 interc_x_by_liq = -avgfit(2)/avgfit(1)
479 interc_y_by_liq = avgfit(2)
480 slope_by_liq = avgfit(1)
481
482 interc_x_by_liq = -avgfit_liq(2)/avgfit_liq(1)
483 interc_y_by_liq = avgfit_liq(2)
484 slope_by_liq = avgfit_liq(1)

```

## Particle detection

The `find_particles` function serves mostly as an interface for the Octave `findpeaks` function and obtains the peaks within certain height and width ranges.

```

1 function [Particles] = find_particles(X,Y,hlims,wlims,mind)
2   if(exist ('OCTAVE_VERSION', 'builtin'))
3     pkg load signal;
4   end
5   Y_pos = Y;
6   Y_pos(find(Y_pos<0))=0;
7   [Particles.maxima,Particles.loc,extra] = findpeaks(Y_pos,'MinPeakHeight',hlims(1),'
      MinPeakWidth',wlims(1),'MaxPeakWidth',wlims(2),'MinPeakDistance',mind);
8   i_valid = find(extra.height<=hlims(2));
9   Particles.pks = extra.height(i_valid);
10  Particles.loc = Particles.loc(i_valid);
11 end

```

## DEP measurements

The scripts in this section are used to measure and analyze the mass jumps for the DEP tests.

### Jump measurement

The `main_DEP` script converts the open loop measurement to a mass shift similarly to the flow-through case, with the difference that no high-pass filter is needed in this case. After that, the jumps corresponding to the release of one or more particles are measured (in height and duration) and saved.

```

1 clear all
2 close all
3
4 if(exist ('OCTAVE_VERSION', 'builtin'))
5   pkg load statistics;
6 end
7
8 cm = 1e-2;
9 um = 1e-6;
10 kHz = 1e3;
11 mV = 1e-3;
12 ms = 1e-3;
13 ng = 1e-12;
14 g = 1e-3;
15
16 %% PARAMETERS %%
17 folder = './dep/h2o';
18 savename = 'h2o-ps8-jumps.txt';
19 %searchstr = {'meas_open*_*_.txt'}; %Starting with meas_open is advised, as the
      script will find the latest sweep files on its own
20 %excludebad = false;
21 %exclude_conditions = {'disturbed'};
22 %exclude_highTC = false;
23 mair = 1267*ng; %empty mass
24 mh2o = 205*ng;
25 dh2o = 0.999*g/cm^3;
26 metOH = 162*ng;
27 detOH = 0.790*g/cm^3;
28
29 psize = 8.13*um;
30
31 Nbars = 10;
32

```

```

33 plottersearch = 'meas_plotter*.txt';
34 sweepsearch = 'meas_sweep*.txt';
35
36 jumpranges = {'meas_plotter27-2507kHz_A4pm_h2o-ps8-dep_20211115_130023.txt' 67.5
    67.85;
37 'meas_plotter27-2507kHz_A4pm_h2o-ps8-dep_20211115_130023.txt' 260 260.26;
38 'meas_plotter37-2507kHz_A4pm_h2o-ps8-dep_20211115_155424.txt' 75.5 75.71;
39 'meas_plotter37-2507kHz_A4pm_h2o-ps8-dep_20211115_155424.txt' 78.08 78.22;
40 'meas_plotter37-2507kHz_A4pm_h2o-ps8-dep_20211115_155424.txt' 105.5 105.85;
41 'meas_plotter37-2507kHz_A4pm_h2o-ps8-dep_20211115_155424.txt' 148.75 149.1;
42 'meas_plotter37-2507kHz_A4pm_h2o-ps8-dep_20211115_155424.txt' 212.9 213.15;
43 'meas_plotter37-2507kHz_A4pm_h2o-ps8-dep_20211115_155424.txt' 259.7 259.88;
44 'meas_plotter37-2507kHz_A4pm_h2o-ps8-dep_20211115_155424.txt' 272.2 272.32;
45 'meas_plotter38-2507kHz_A4pm_h2o-ps8-dep_20211115_160154.txt' 9.35 9.5;
46 'meas_plotter38-2507kHz_A4pm_h2o-ps8-dep_20211115_160154.txt' 38.2 38.6;
47 'meas_plotter38-2507kHz_A4pm_h2o-ps8-dep_20211115_160154.txt' 200.8 200.96;
48 'meas_plotter38-2507kHz_A4pm_h2o-ps8-dep_20211115_160154.txt' 244.2 244.35;
49 'meas_plotter38-2507kHz_A4pm_h2o-ps8-dep_20211115_160154.txt' 246.5 246.64;
50 'meas_plotter38-2507kHz_A4pm_h2o-ps8-dep_20211115_160154.txt' 262.75 263;
51 'meas_plotter38-2507kHz_A4pm_h2o-ps8-dep_20211115_160154.txt' 279.15 279.4;
52 'meas_plotter38-2507kHz_A4pm_h2o-ps8-dep_20211115_160154.txt' 283.35 283.5;
53 'meas_plotter38-2507kHz_A4pm_h2o-ps8-dep_20211115_160154.txt' 290 290.3;
54 'meas_plotter39-2507kHz_A4pm_h2o-ps8-dep_20211115_160953.txt' 34.13 34.34;
55 'meas_plotter39-2507kHz_A4pm_h2o-ps8-dep_20211115_160953.txt' 41.5 41.72;
56 'meas_plotter39-2507kHz_A4pm_h2o-ps8-dep_20211115_160953.txt' 83.1 83.3;
57 'meas_plotter39-2507kHz_A4pm_h2o-ps8-dep_20211115_160953.txt' 116.3 116.6;
58 'meas_plotter39-2507kHz_A4pm_h2o-ps8-dep_20211115_160953.txt' 156.65 156.85;
59 'meas_plotter39-2507kHz_A4pm_h2o-ps8-dep_20211115_160953.txt' 191.2 191.41;
60 'meas_plotter39-2507kHz_A4pm_h2o-ps8-dep_20211115_160953.txt' 280.45 280.65;
61 'meas_plotter40-2507kHz_A4pm_h2o-ps8-dep_20211115_161938.txt' 47.8 47.96;
62 'meas_plotter40-2507kHz_A4pm_h2o-ps8-dep_20211115_161938.txt' 119.7 119.9;
63 'meas_plotter40-2507kHz_A4pm_h2o-ps8-dep_20211115_161938.txt' 237.5 237.61;
64 'meas_plotter40-2507kHz_A4pm_h2o-ps8-dep_20211115_161938.txt' 277.65 277.9
65 };
66
67 %%%%%%%%%%%%%
68
69 homefolder=pwd;
70 addpath(pwd); %In this way we can work on any folder
71
72 cd(folder);
73
74 sweeplist = ls2cell(sweepsearch);
75 for i=1:length(sweeplist)
76     Buffer = read_simple(sweeplist{i});
77
78     Buffer.Fits = {};
79     Sweeps{i} = Buffer;
80 end
81
82 Mass_shifts = [];
83 Release_times = [];
84
85 for i=1:size(jumpranges,1)
86     %parameters
87     fitsize = 10*kHz; %for phase fit
88
89     if ~strcmp(jumpranges{i,1},Buffer.filename)
90         Buffer = read_simple(jumpranges{i,1});
91
92         i_sweep = intersect(sfind(Sweeps,'device',Buffer.device),sfind(Sweeps,'condition',
            strep(Buffer.condition,'-CUT','')));

```

```

93     timestamps = cellfun('getfield',Sweeps(i_sweep),repmat({'timestamp'},1,length(
94     i_sweep)));
95     [~,i_sweep] = min(abs(timestamps-Buffer.timestamp)); %index of sweep
96     Buffer.i_sweep = i_sweep;
97     current_Sweep = Sweeps{i_sweep};
98
99     i_fit = sfind(current_Sweep.Fits,'X0',Buffer.X0);
100     if isempty(i_fit)
101         current_Sweep.Fits{end+1} = phase_fit(current_Sweep,Buffer.X0,fitsize); %
102         phase_fit
103         i_fit = length(current_Sweep.Fits);
104     end
105     Buffer.i_fit = i_fit;
106
107     current_Fit = current_Sweep.Fits{i_fit};
108
109     Buffer.Yfreq = current_Fit.X0-(Buffer.Yphase-current_Fit.phase0)/current_Fit.
110     phasepoly(1);
111
112     current_conds = strsplit(Buffer.condition,{'+', '-'});
113     switch current_conds{1}
114     case 'h2o'
115         n_liq = 5;
116         Buffer.m0 = mair+mh2o;
117         Buffer.dliquid = dh2o;
118     case 'etOH'
119         n_liq = 1;
120         Buffer.m0 = mair+metOH;
121         Buffer.dliquid = detOH;
122     case '25etOH'
123         n_liq = 4;
124         Buffer.m0 = mair+0.25*metOH+0.75*mh2o;
125         Buffer.dliquid = 0.25*detOH+0.75*dh2o;
126     case '50etOH'
127         n_liq = 3;
128         Buffer.m0 = mair+0.5*metOH+0.5*mh2o;
129         Buffer.dliquid = 0.5*detOH+0.5*dh2o;
130     case '75etOH'
131         n_liq = 2;
132         Buffer.m0 = mair+0.75*metOH+0.25*mh2o;
133         Buffer.dliquid = 0.75*detOH+0.25*dh2o;
134     end
135
136     Buffer.Ypmass = -2*Buffer.m0*(Buffer.Yfreq-current_Fit.X0)./(current_Fit.X0); %
137     this is only actually valid for the peaks!!
138 end %else USA IL BUFFER PRECEDENTE
139
140 current_range = intersect(find(jumpranges{i,2}<=Buffer.X),find(Buffer.X<=jumpranges{
141     i,3}));
142 Ypmass_current = Buffer.Ypmass(current_range);
143 X_current = Buffer.X(current_range);
144
145 [current_min,current_imin] = min(Ypmass_current);
146 [current_max,current_imax] = max(Ypmass_current);
147
148 Mass_shifts(i) = current_max-current_min;
149 Release_times(i) = X_current(current_imin)-X_current(current_imax);
150
151 %check for step direction
152 if(Release_times(i)<0)
153     error('Wrong step!')
154 end

```

```

150
151 figure()
152 plot(Buffer.X,Buffer.Ypmass/ng)
153 hold on
154 box on
155 plot(X_current(current_imax),current_max/ng,'kv')
156 title({'DEP mass shift - stop+release',strcat('Device:A4 - Suspension:ps8 in H_2O'),
        strcat('Measurement #',Buffer.ID,'@',num2str(Buffer.X0/kHz),'kHz')},'FontSize',15)
157 xlabel('Time(s)','FontSize',15)
158 ylabel('Buoyant mass(ng)','FontSize',15)
159 %print(current_savename,'-depsc')
160
161 end
162
163 M = [Mass_shifts',Release_times'];
164 dlmwrite(savename,M,','',0,0)
165
166 cd(homefolder);

```

## Data analysis

The main\_DEP\_post script collects all the saved informations on the DEP events and, among other things, obtains the mass distributions and their lognormal fits similarly to the flow-through case.

```

1 clear all
2 close all
3
4 if(exist ('OCTAVE_VERSION', 'builtin'))
5     pkg load statistics;
6 end
7
8 cm = 1e-2;
9 um = 1e-6;
10 kHz = 1e3;
11 mV = 1e-3;
12 ms = 1e-3;
13 ng = 1e-12;
14 pg = 1e-15;
15 g = 1e-3;
16 mm = 1e-3;
17
18 folder = '../dep/h2o';
19 datafile = 'h2o-ps8-data.txt';
20
21 titlepre = 'A4-h2o-ps8';
22 savepre = 'A4-h2o-ps8';
23
24 Nbars = 7;
25
26 homefolder = pwd;
27 addpath(pwd)
28 cd(folder)
29
30 M = dlmread(datafile,','');
31
32 ranges = [];
33 jumps = [];
34 halftimes = [];
35 speeds = [];
36 pressures = [];
37 Vranges = [];
38 posranges = [];

```



```

39
40 counts = M(:,16);
41
42 for i = 1:length(counts)
43     if counts(i)>=2&&counts(i)<=6
44         ranges = [ranges;repmat(M(i,[1,2]),counts(i),1)];
45         jumps = [jumps;repmat(M(i,3)/counts(i),counts(i),1)];
46         halftimes = [halftimes;repmat(M(i,4),counts(i),1)];
47         pressures = [pressures;repmat(M(i,[5:8]),counts(i),1)];
48         Vranges = [Vranges;repmat(M(i,[12,13]),counts(i),1)];
49         posranges = [posranges;repmat(M(i,[15,17]),counts(i),1)];
50     elseif counts(i)>6
51         warning('too many particles,skipped a measurement')
52     else
53         ranges = [ranges;M(i,[1,2])];
54         jumps = [jumps;M(i,3)];
55         halftimes = [halftimes;M(i,4)];
56         pressures = [pressures;M(i,[5:8])];
57         Vranges = [Vranges;M(i,[12,13])];
58         posranges = [posranges;M(i,[15,17])];
59     end
60 end
61
62 speeds = (125*um)./halftimes;
63
64 %Full jumps (ignoring particle count)
65 m_ranges = M(:,[1,2]);
66 m_jumps = M(:,3);
67 m_halftimes = M(:,4);
68 m_pressures = M(:,[5:8]);
69 m_Vranges = M(:,[12,13]);
70 m_posranges = M(:,[12,13]);
71 m_speeds = (125*um)./m_halftimes;
72
73 m_jump_fit = polyfit(counts(3:end),m_jumps(3:end),1);
74 m_jump_fit_cut = polyfit(counts(find(counts<=7)),m_jumps(find(counts<=7)),1);
75
76 figure()
77 hold on
78 box on
79 plot(counts(3:end),m_jumps(3:end)/pg,'x','Color','b','LineWidth',1.5,'HandleVisibility','off')
80 plot(1:max(counts(3:end)),polyval(m_jump_fit,1:max(counts(3:end)))/pg,'b','LineWidth',1,'DisplayName','fit of all the data')
81 plot(1:max(counts(3:end)),polyval(m_jump_fit_cut,1:max(counts(3:end)))/pg,'b--','LineWidth',1,'DisplayName','fit of the data with N<8')
82 title({'DEP Mass shifts vs. # of stopped particles','Device:A4 - Suspension:ps8 in H_2O','P_1=30mbar - P_2=15mbar - P_3=40mbar - P_4=0'},'FontSize',15)
83 xlabel('# of particles','FontSize',15)
84 ylabel('Mass shift(pg)','FontSize',15)
85 xlim([1,max(counts(3:end))])
86 legend('FontSize',13)
87 print(strcat(savepre,'_shift_v_N-dep.eps'),'-depsc')
88
89 [pks_m_logn,pks_s_logn] = logn_fit(jumps);
90 pks_mode = exp(pks_m_logn-pks_s_logn^2)
91
92 figure()
93 hold on
94 box on
95 hist(jumps/pg,Nbars,'facecolor','w');
96 xtemp = linspace(min(jumps),max(jumps),100);

```

```

97 %ytemp = (length(jumps))*(max(jumps)-min(jumps))*lognpdf(xtemp,pks_m_logn,pks_s_logn);
98 ytemp = (mean(histc(jumps,linspace(min(jumps),max(jumps),Nbars+1)))/mean(lognpdf(xtemp
    ,pks_m_logn,pks_s_logn)))*lognpdf(xtemp,pks_m_logn,pks_s_logn);
99 plot(xtemp/pg,ytemp)
100 title({'DEP Mass Shifts Distribution','Device:A4 - Suspension:ps8 in H_2O','P_1=30mbar
    - P_2=15mbar - P_3=40mbar - P_4=0'},'FontSize',15)
101 xlabel('Mass Shift(pg)','FontSize',15)
102 ylabel('# of events','FontSize',15)
103 xlim([min(jumps/pg),max(jumps/pg)])
104 ylim([0,13])
105 print(strcat(savepre,'_pkdistr-dep.eps'),'-depsc')
106 %close
107
108 figure()
109 hold on
110 box on
111 jumps_1 = m_jumps(find(counts==1));
112 [pks_m_logn,pks_s_logn] = logn_fit(jumps_1);
113 hist(jumps_1/pg,Nbars,'facecolor','w');
114 xtemp = linspace(min(jumps_1),max(jumps_1),100);
115 %ytemp = (length(jumps))*(max(jumps)-min(jumps))*lognpdf(xtemp,pks_m_logn,pks_s_logn);
116 ytemp = (mean(histc(jumps_1,linspace(min(jumps_1),max(jumps_1),Nbars+1)))/mean(lognpdf
    (xtemp,pks_m_logn,pks_s_logn)))*lognpdf(xtemp,pks_m_logn,pks_s_logn);
117 plot(xtemp/pg,ytemp)
118 title({'DEP Single Particle Mass Shifts Distribution','Device:A4 - Suspension:ps8 in
    H_2O','P_1=30mbar - P_2=15mbar - P_3=40mbar - P_4=0'},'FontSize',15)
119 xlabel('Mass Shift(pg)','FontSize',15)
120 ylabel('# of events','FontSize',15)
121 xlim([min(jumps_1/pg),max(jumps_1/pg)])
122 ylim([0,6])
123 print(strcat(savepre,'_pkdistr1-dep.eps'),'-depsc')
124 %close
125
126 figure()
127 hold on
128 box on
129 done_legend = [false,false];
130 for i=3:length(speeds)
131     if Vranges(i,1)==Vranges(i,2)
132         if ~done_legend(1)
133             plot(Vranges(i,1),speeds(i)/mm,'x','Color',[0.9290 0.6940 0.1250],'LineWidth'
    ,1.5,'DisplayName','Unstable stop')
134             done_legend(1)=true;
135         else
136             plot(Vranges(i,1),speeds(i)/mm,'x','Color',[0.9290 0.6940 0.1250],'LineWidth'
    ,1.5,'HandleVisibility','off')
137         end
138     else
139         if ~done_legend(2)
140             plot(Vranges(i,1),speeds(i)/mm,'x','Color','r','LineWidth',1.5,'DisplayName','
    Stop')
141             plot(Vranges(i,2),speeds(i)/mm,'x','Color','g','LineWidth',1.5,'DisplayName','
    Release')
142             plot(Vranges(i,:),[speeds(i),speeds(i)]/mm,'y','LineWidth',1,'HandleVisibility',
    'off') %keeping only 30 15 40 0
143             done_legend(2)=true;
144         else
145             plot(Vranges(i,1),speeds(i)/mm,'x','Color','r','LineWidth',1.5,'HandleVisibility'
    ,',off')
146             plot(Vranges(i,2),speeds(i)/mm,'x','Color','g','LineWidth',1.5,'HandleVisibility'
    ,',off')

```

```

147     plot(Vranges(i,:),[speeds(i),speeds(i)]/mm,'y','LineWidth',1,'HandleVisibility',
148           'off')
149     end
150 end
151 title({strcat(titlepre,'-0.L. @2507kHz-DEP Release speeds vs. Release tensions'),'P1
152         =30mbar, P2=15mbar, P3=40mbar, P4=0'})
153 xlabel('Tension(V)')
154 ylabel('Release speed(mm/s)')
155 legend('location','eastoutside')
156 %print(strcat(savepre,'_speed-dep.eps'),'--depsc')
157 close
158
159 figure()
160 hold on
161 box on
162 title({'DEP Tensions','Device:A4 - Suspension:ps8 in H_2O','P_1=30mbar - P_2=15mbar -
163         P_3=40mbar - P_4=0'},'FontSize',15)
164 i_unstable = find(Vranges(:,1)==Vranges(:,2));
165 i_stable = find(Vranges(:,1)~=Vranges(:,2));
166 h=bar(i_unstable(3:end)-2,Vranges(i_unstable(3:end),1),'DisplayName','Unstable Stop');
167 set(h,'facecolor',[0.9290 0.6940 0.1250]);
168 h=bar(i_stable-2,[Vranges(i_stable,2), Vranges(i_stable,1)-Vranges(i_stable,2)],'
169         stacked');
170 set(h(1),'facecolor','g','DisplayName','Release');
171 set(h(2),'facecolor','r','DisplayName','Stop');
172 xlabel('Event #','FontSize',15)
173 ylabel('DEP Tension(V)','FontSize',15)
174 legend('location','south','FontSize',13)
175 print('Vdep.eps','--depsc')
176 %close
177
178 cd(homefolder)

```

## References

- [1] M. L. R. Silvan Schmid, Luis Guillermo Villanueva, *Fundamentals of Nanomechanical Resonators*. Springer, Cham, 1 ed., 2016.
- [2] T. P. Burg and S. R. Manalis, “Suspended microchannel resonators for biomolecular detection,” *Applied Physics Letters*, vol. 83, no. 13, pp. 2698–2700, 2003.
- [3] T. P. Burg, M. Godin, S. M. Knudsen, W. Shen, G. Carlson, J. S. Foster, K. Babcock, and S. R. Manalis, “Weighing of biomolecules, single cells and single nanoparticles in fluid,” *Nature*, vol. 446, pp. 1066–1069, Apr 2007.
- [4] A. D. Pastina and L. G. Villanueva, “Suspended micro/nano channel resonators: a review,” *Journal of Micromechanics and Microengineering*, vol. 30, p. 043001, feb 2020.
- [5] Y. Weng, F. F. Delgado, S. Son, T. P. Burg, S. C. Wasserman, and S. R. Manalis, “Mass sensors with mechanical traps for weighing single cells in different fluids,” *Lab Chip*, vol. 11, pp. 4174–4180, 2011.
- [6] T. Z. Jubery, S. K. Srivastava, and P. Dutta, “Dielectrophoretic separation of bioparticles in microdevices: a review,” *Electrophoresis*, vol. 35, pp. 691–713, mar 2014.
- [7] M. Gagino, G. Katsikis, S. Olcum, L. Viro, M. Cochet, A. Thuaire, S. R. Manalis, and V. Agache, “Suspended nanochannel resonator arrays with piezoresistive sensors for high-throughput weighing of nanoparticles in solution,” *ACS Sensors*, vol. 5, no. 4, pp. 1230–1238, 2020. PMID: 32233476.
- [8] B. Cetin and D. Li, “Dielectrophoresis in microfluidics technology,” *Electrophoresis*, vol. 32, pp. 2410–2427, sep 2011.
- [9] M. Evander, L. Johansson, T. Lilliehorn, J. Piskur, M. Lindvall, S. Johansson, M. Almqvist, T. Laurell, and J. Nilsson, “Noninvasive acoustic cell trapping in a microfluidic perfusion system for online bioassays,” *Analytical Chemistry*, vol. 79, no. 7, pp. 2984–2991, 2007. PMID: 17313183.
- [10] R. M. Johann, “Cell trapping in microfluidic chips,” *Analytical and Bioanalytical Chemistry*, vol. 385, pp. 408–412, Jun 2006.
- [11] R. Calmo, *Monolithic glass suspended microchannel resonators for bead-based assay integration*. PhD thesis, Politecnico di Torino, 2020.
- [12] R. Calmo, A. Lovera, S. Stassi, A. Chiadò, D. Scaiola, F. Bosco, and C. Ricciardi, “Monolithic glass suspended microchannel resonators for enhanced mass sensing of liquids,” *Sensors and Actuators B: Chemical*, pp. 298–303, 2019.
- [13] J. L. Arlett, E. B. Myers, and M. L. Roukes, “Comparative advantages of mechanical biosensors,” *Nature Nanotechnology*, vol. 6, pp. 203–215, Apr 2011.
- [14] R. Osellame, H. Hoekstra, G. Cerullo, and M. Pollnau, “Femtosecond laser microstructuring: an enabling tool for optofluidic lab-on-chips,” *Laser & Photonics Reviews*, vol. 5, no. 3, pp. 442–463, 2011.
- [15] Y. Bellouard, “The femtoprint project,” *Journal of Laser Micro/Nanoengineering*, vol. 7, pp. 1–10, 02 2012.
- [16] D.V.Land, *The use of the Allan deviation for the identification and measurement of noise and drift in measurement data*. PhD thesis, University of Glasgow, 2014.